University of New Mexico
UNM Digital Repository

Nuclear Engineering ETDs | Engineering ETDs

9-3-2013

# An ionization chamber for fission fragment analysis

Drew Mader

Follow this and additional works at: https://digitalrepository.unm.edu/ne_etds

Recommended Citation
Mader, Drew. "An ionization chamber for fission fragment analysis." (2013). https://digitalrepository.unm.edu/ne_etds/33

This Thesis is brought to you for free and open access by the Engineering ETDs at UNM Digital Repository. It has been accepted for inclusion in Nuclear Engineering ETDs by an authorized administrator of UNM Digital Repository. For more information, please contact disc@unm.edu.

Drew Mader

*Candidate*

Chemical & Nuclear Engineering

*Department*

This thesis is approved, and it is acceptable in quality and form for publication:

*Approved by the Thesis Committee:*

Dr. Adam Hecht, Chairperson

Dr. Robert Busch

Dr. Cassiano de Oliveria

**An Ionization Chamber for Fission Fragment Analysis**

By

Drew M. Mader

Bachelor of Science – Physics 2011

University of St. Thomas

Submitted in Partial Fulfillment of the
Requirements for the Degree of

**Master of Science**

**Nuclear Engineering**

The University of New Mexico
Albuquerque, New Mexico

**June 2013**

## ACKNOWLEDGEMENTS

I would like to first thank all my friends and family who have given me support throughout my life. I would also like to thank my committee members Dr. Robert Busch, Dr. Cassiano de Oliveria, and Dr. Adam Hecht for not only being part of my committee, but also for their various support throughout my graduate degree.

Individually, I deeply thank my adviser Dr. Adam Hecht for giving me the opportunity to work on this project and the numerous amounts of support, help, and enjoyment he has brought me over the past two years. Also, I thank Rick Blakeley, my co-worker and great friend, for his significant help and input during this project. Finally, I thank Mr. Ken Carpenter for his deep knowledge and troubleshooting when it comes to radiation detectors, signal processing, and electronics. These three individuals were essential to my and this project's success.

**An Ionization Chamber for Fission Fragment Analysis**

**by**

**Drew Mader**

**B.Sc., Physics, University of St. Thomas, 2011**

**M.Sc., Nuclear Engineering, University of New Mexico, 2013**

## ABSTRACT

Fission fragments play a pivotal role in understanding the entire nuclear fission process, and their effects are widespread to all applications involving nuclear fission: reactor design and maintenance, waste removal, active and passive integration of nuclear materials, simulations, and the fundamental theories of fission. Currently, experimental data on the characteristic properties of fission fragment distributions is lacking at variable neutron energies as well as with sufficient uncertainty, and therefore better experimental data is desired.

To achieve this goal, the Spectrometer for Ion Detection in Fission Research project (SPIDER) is being designed which uses high resolution measurements and event-by-event analysis to increase the amount of nuclear fission data available [White]. As a collaborator, we are building and testing an ionization chamber to be used for the SPIDER project which will ultimately take place at the LANSCE facility at Los Alamos National Laboratory.

A full spectrum of the pertinent variables dictating the functionality of the ionization chamber have been investigated and characterized where an energy resolution of just below 1.5% was achieved.

**Table of Contents**

**An Ionization Chamber for Fission Fragment Analysis**

List of Figures ..... viii
List of Tables ..... x

**Chapter 1 – Introduction** ..... **1**

**Chapter 2 – Theory** ..... **3**
2.1. The 2v-2E Method ..... 3
2.2. The Time-of-Flight Measurement ..... 5
2.3.1. The Energy Measurement ..... 6
2.3.2. Background ..... 6
2.3.3. Operating Characteristics of Ionization Chambers ..... 8
2.3.4. Statistics of Ionization ..... 9
2.3.5. Energy Resolution ..... 11
2.4. Mass Resolution ..... 13
2.5. The Atomic Number Measurement ..... 15

**Chapter 3 – Detector Characteristics and Construction** ..... **21**
3.1. Drift Velocity ..... 21
3.2.1. Ion Interactions ..... 22
3.2.1. Electron Capture ..... 23
3.2.3. Recombination ..... 25
3.2.4. Diffusion ..... 28
3.2.5. Space Charge ..... 30
3.2.6. Conclusions ..... 31
3.3. The Ionization Chamber Pulse Height ..... 31
3.4.1. The Frisch-gridded Ionization Chamber Pulse Height ..... 37
3.4.2. Frisch Grid ..... 40
3.5.1. Detector Construction and Components ..... 42
3.5.2. Noise ..... 47
3.6. Guard Rings ..... 49
3.7.1. SIMION 8.1 ..... 50

3.7.2. Electric Field ..... 50
3.7.3. Number of Guard Rings ..... 54
**Chapter 4 – Experiment and Results** ..... **55**
4.1. Experiment Introduction ..... 55
4.2. Experimental System ..... 55
4.3. Dead Layer ..... 57
4.4. Peak Drift ..... 60
4.5. Gas Flow ..... 61
4.6. Lateral Acceptance ..... 62
4.7. Shaping Time ..... 64
4.8. Electric Field ..... 69
4.9. Pressure ..... 71
4.10. Bragg Curve Spectroscopy ..... 74
**Chapter 5 – Conclusions and Future Work** ..... **76**
5.1. Conclusions ..... 76
5.2. Energy Resolution ..... 77
5.3. Pressure Dependence ..... 77
5.4. Isobutane ..... 77
5.5. Window ..... 78
**References** ..... **79**
**Appendices** ..... **83**
**Appendix A – Charge Sensitive Preamplifiers** ..... **84**
A.1. Properties ..... 84
A.2. Bragg Curve Spectroscopy ..... 85
**Appendix B – Pulse and Current Mode of Ionization Chamber Operation** ..... **87**
B.1. Introduction ..... 87
B.2. Pulse Mode ..... 87
B.3. Current Mode ..... 88

## List of Figures

FIGURE 1: 2V-2E SPECTROMETER .....5

FIGURE 2: TRANSVERSE IC .....7

FIGURE 3: I-V CURVE .....9

FIGURE 4: THE BRAGG CURVES FOR THREE DIFFERENT ENERGY ALPHA PARTICLES.....16

FIGURE 5: OVERLAPPED BRAGG CURVES .....17

FIGURE 6: BRAGG CURVES FOR THREE DIFFERENT ATOMIC CHARGED PARTICLES .....18

FIGURE 7: THE BRAGG PEAK VS. DEPOSITED ENERGY.....20

FIGURE 8: THE DRIFT VELOCITY OF P-10 GAS.....22

FIGURE 9: CIRCUITRY USED FOR AN IC.....32

FIGURE 10: THE OUTPUT VOLTAGE AS A FUNCTION OF TIME .....36

FIGURE 11: THE GEOMETRICAL AND ELECTRIC LAYOUT OF A FRISCH-GRIDDED IC .....38

FIGURE 12: THE OUTPUT VOLTAGE AS A FUNCTION OF TIME IN A FRISCH-GRIDDED IC.....39

FIGURE 13: OUR IC .....42

FIGURE 14: A CROSS-SECTIONAL VIEW OF OUR IC.....43

FIGURE 15: TOP VIEW OF OUR IC.....44

FIGURE 16: THE FRISCH GRID .....45

FIGURE 17: THE EXTERNAL SYSTEM USED TO HOUSE THE IC.....46

FIGURE 18: THE EXTERNAL SYSTEM USED TO OPERATE THE IC .....47

FIGURE 19: TOP-DOWN VIEW OF THE IC.....47

FIGURE 20: THE SIGNAL CABLE.....48

FIGURE 21: DIRECTLY HOOKED UP PREAMPLIFER.....49

FIGURE 22: THE ELECTRIC FIELD LINES .....51

FIGURE 23: ELECTRIC FIELD RATIO IN THE CATHODE-FRISCH GRID REGION.....52

FIGURE 24: ELECTRIC FIELD RATIO IN THE FRISCH GRID-ANODE REGION.....53

FIGURE 25: THE SIGNAL PROCESSING SYSTEM.....57

FIGURE 26: THE DEAD LAYER OF THE IC. ....58
FIGURE 27: UNCERTAINTIES FROM THE DEAD LAYER ....59
FIGURE 28: ENERGY RESOLUTION VS. E/P FOR GAS FLOW AND NO GAS FLOW ....62
FIGURE 29: COUNT RATE VS. DISTANCE FROM CENTER ....63
FIGURE 30: FWHM VS. DISTANCE FROM CENTER ....63
FIGURE 31: NOISE VS. SHAPING TIME ....65
FIGURE 32: CHANNEL NUMBER VS. *E/P* AT VARIOUS SHAPING TIMES ....66
FIGURE 33: THE ENERGY RESOLUTION VS. SHAPING TIME ....67
FIGURE 34: ENERGY RESOLUTION VS. E/P AT 2 AND 3 μS SHAPING TIMES ....68
FIGURE 35: THE I-V CURVE OF OUR IC ....69
FIGURE 36: THE ENERGY RESOLUTION VS. ELECTRIC FIELD ....70
FIGURE 37: CHANNEL NUMBER VS. PRESSURE AT DIFFERENT ELECTRIC FIELD RATIOS ....71
FIGURE 38: CHANNEL NUMBER VS. PRESSURE FOR TWO ALPHA PARTICLES ....72
FIGURE 39: THE ENERGY RESOLUTION VS. PRESSURE ....73
FIGURE 40: BRAGG CURVE SPECTROSCOPY ....75
FIGURE 41: VOLTAGE PULSE FROM PREAMPLIFER ....86
FIGURE 42: PULSE MODE OF OPERATION ....88

## List of Tables

TABLE 1: THE RECOMBINATION COEFFICIENTS OF VARIOUS GASES .....27

TABLE 2: EXPERIMENTAL SOURCES USED .....56

## Chapter 1

## 1. Introduction

---

Nuclear fission is the process in which a heavy nucleus breaks apart into various particles accompanied by the release of large amounts of energy. Generally in *neutron-induced* fission reactions, the heavy nucleus breaks apart into two lighter nuclei, called fission fragments, among other things. To date, there is very little data with sufficient uncertainty on the complete characterization of the fission fragments for varying heavy nuclei and incident energy neutron. Better fission fragment data would be beneficial in most applications involving nuclear fission: decay heating in nuclear reactors, nuclear waste maintenance, simulations, and the fundamental theories of fission itself.

We propose to use a dual-arm fission fragment spectrometer to study the important parameters of fission fragments: energy, atomic number, and mass. The spectrometer is based on the 2v-2E method [Boucheneb, 1989], where first the transmission time-of-flight of both fission fragments is used to measure their respective velocities, followed by an energy measurement from a Frisch-gridded ionization chamber. These two values allow one to infer the mass of a fission fragment. The novel goal of this experiment is to keep all uncertainties to an absolute minimum so as to achieve a *less than one amu mass resolution* for *both* fission fragments. The fission fragments' atomic charge will also be determined in the ionization chamber based on their energy and range in the detector.

The neutron beamline at the Los Alamos Neutron Science Center (LANSCE)

will provide neutron energies from the milli-eV to keV range. Initial measurements will focus on the thermal fission of U-235 and Pu-239 targets, where high resolution data is needed and most beneficial [White].

The purpose of this work is to design, build, and test an ionization chamber with low uncertainty to be in accordance with the *less than one amu uncertainty* goal for both fission fragments. Initial tests with alpha particles will be used to characterize the ionization chamber, where an energy resolution of less than 1.25% is desired for the alpha particles. The energy resolution is defined as the full width at half maximum over the centroid (this is not to be confused with the mass resolution which is simply the uncertainty in the mass measurement).

# Chapter 2

# Theory

---

## 2.1. The 2v-2E Method

The fission fragment's time-of-flight measurement, which occurs at high vacuum, is measured using thin foils, electrostatic mirrors, and microchannel plate detectors. Figure 1 shows one "arm" of the proposed spectrometer (the final design will contain eight arms to increase the efficiency). Located in the middle of one arm is an actinide which will be bombarded by neutrons to induce fission and produce two fission fragments. Each fragment will first pass through a very thin carbon foil where it rips off some electrons in the process. In our case, these foils are 100 $\mu g/cm^2$ thin carbon foils; the size was chosen to minimize uncertainty in the energy loss of the fission fragment. These electrons, which are emitted in a 4π-direction, will see an electric field produced by the electrostatic mirror, which is simply a set of biased wires forming a grid, and be pushed toward a microchannel plate timing detector (see [Kozulin] for a more information on the electrostatic mirrors). This microchannel plate provides the START signal for the time-of-flight measurement. As this is occurring, the fission fragment passes through the electrostatic mirror and interacts with a replica of the previous setup (although in the reverse direction); more electrons are emitted and subsequently bent down to the second microchannel plate detector forming the STOP signal for the time-of-flight measurement. This time-of-flight, *t*, combined with a known distance, *l*, gives the average velocity of the fission fragment, *v*,

$$v = \frac{l}{\mathrm{t}} \qquad \text{Eq. 1}$$

The fission fragment then enters the gaseous portion of the spectrometer, a Frisch-gridded ionization chamber, where its energy, *E,* and atomic number are measured. This allows one to determine the fission fragment's mass, *m,* by

$$m = 2E\left(\frac{t}{l}\right)^2 \qquad \text{Eq. 2}$$

The main aspect of this work is to keep the uncertainty in the mass, $\delta_m$, to be less than one amu. $\delta_m$ is defined as

$$\delta_m{}^2 = (\frac{dm}{dE}\delta_E)^2 + (\frac{dm}{dl}\delta_{\mathrm{l}})^2 + (\frac{dm}{dt}\delta_{\mathrm{t}})^2 \qquad \text{Eq. 3}$$

where $\delta_E, \delta_{\mathrm{l}}$, and $\delta_t$ are the uncertainties in the energy, distance, and time respectively. The uncertainty in the mass is commonly given as the fractional uncertainty:

$$\frac{\delta_m}{\mathrm{m}} = \sqrt{\left(\frac{\delta_E}{\mathrm{E}}\right)^2 + \left(2\frac{\delta_l}{l}\right)^2 + \left(2\frac{\delta_t}{\mathrm{t}}\right)^2} \qquad \text{Eq. 4}$$

Considering that one can generally keep $\delta_l$ and $\delta_t$ relatively low, $\delta_{\mathrm{E}}$ becomes the dominant factor in obtaining the lowest mass resolution possible, and therefore the ionization chamber is perhaps the most important part of this spectrometer.

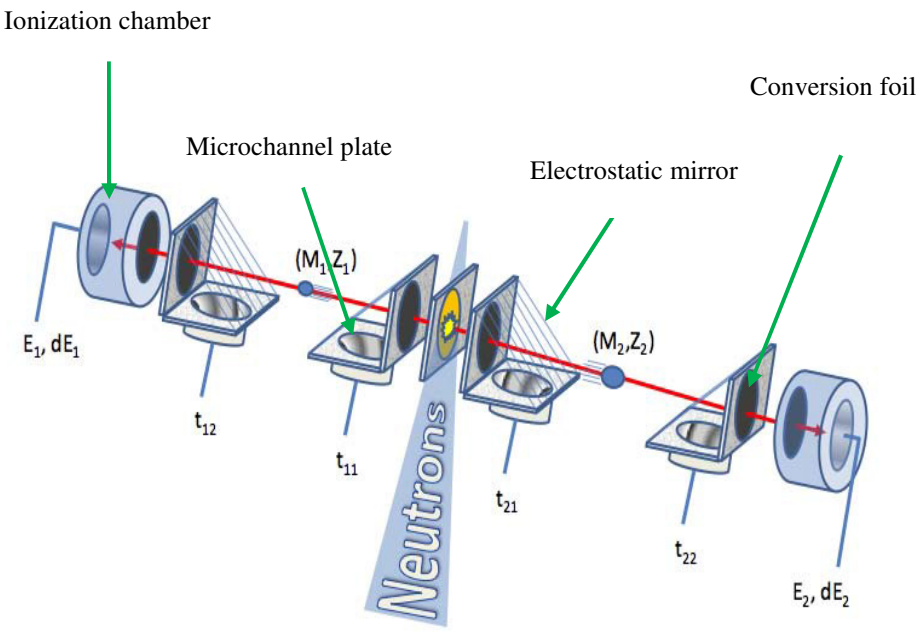



Figure 1: One arm of the proposed fission fragment spectrometer

### 2.2. The Time-of-Flight Measurement

The microchannel plate detectors are the key component to the time-of-flight measurement, and their use in this experiment is based on their low uncertainty in fast timing applications. Microchannel plates were first fully implemented around 1960 [Wiza], and their fundamental operation is somewhat similar to that of proportional counters (the reader is directed to [Wiza] for a better understanding of their operation and functionality). Uncertainties in single microchannel plate applications, $\delta_t$, can be easily obtained under 100 ps, with achieved uncertainties for similar 2v-2E measurements being consistently around 65-80 ps [Starzecki, Kosev, D'Erasmo] for heavy ions ranging from alpha particles to fission fragments. Initial tests with the microchannel plate detectors used by our collaborators at Los Alamos National Laboratory have achieved a $\delta_t$ of about

80 ps. After optimization, hopefully this value can be lowered to the 65 ps value others have accomplished.

### 2.3.1. The Energy Measurement Introduction

An ionization chamber (IC) will be the detector used for the energy and atomic number measurement for this 2v-2E method and will be the majority of this discussion. Other 2v-2E methods have used solid state surface barrier detectors [Kozulin] for their energy measurement; however their uncertainty significantly increases with heavy ions (e.g. fission fragments) [Muller]. That fact, combined with the large solid angle easily obtainable with ICs, often times make them much more practical than solid state detectors and is thus why ICs are being used for this spectrometer.

### 2.3.2. Background

An IC is one of the simplest gas-filled detectors that use the phenomenon of gas ionization to indirectly measure the energy of an ionizing particle. ICs were first developed in the late $19^{th}$ century [Wilkinson] and are still commonly used today due to their simplistic nature and versatility. ICs are most generally used as portable dose meters as well as in applications where energy and timing information is desired. More recently, ICs has been used in the area known as *Bragg curve spectroscopy* [Gruhn], where the reconstruction of the Bragg curve is desired for atomic charge information.

The simplest version of an IC consists of two electrodes, of differing voltages, separated by some distance which is filled with gas (Figure 2); an obvious electric field is

established between the electrodes. When an ionizing particle enters the region between the electrodes, dubbed the *active region*, it releases its energy by ionizing the gas molecules and therefore creates numerous electron-ion pairs. As both of these charged particles drift in the presence of the electric field, they induce a charge on their respective electrodes; this charge is the basis for a measured signal.

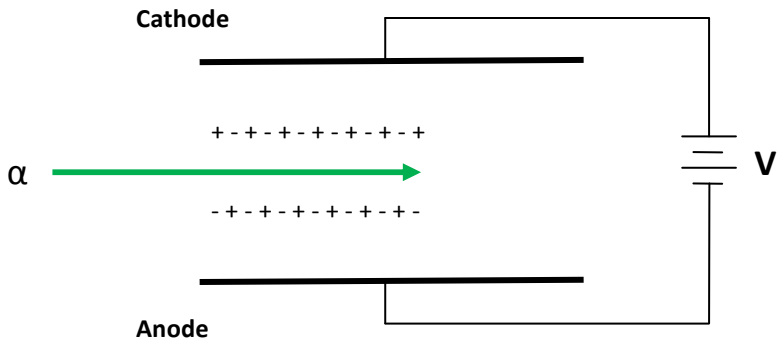



Figure 2: The simplest design of a transverse ionization chamber

The three main types of geometries used for ICs are the coaxial, transverse, and axial geometries. A coaxial IC typically has a very thin collecting electrode surrounded by a grounded chamber resembling the geometry of a coaxial cable. A transverse IC (Figure 2) has its electric field perpendicular to direction of the ionizing particle, whereas the axial chamber has its field parallel to this direction. Each design has their specific advantage for different applications. The following experiment uses the axial geometry, and therefore the rest of the discussion will be restricted to this type, however much of the theory still applies to the other geometries.

### 2.3.3. Operating Characteristics of Ionization Chambers

All gas-filled detectors fundamentally operate the same way: an ionizing particle enters the active region of the detector where it loses energy by ionization producing a number of electron-ion pairs proportional to its incident energy; these are called the *primary ionizations*. The electrons and ions then drift toward their respective electrodes because of the established electric field within the detector. As this voltage difference between the electrodes is increased (above what is used for IC), the electrons and ions themselves can gain enough energy to ionize more of the gas and thus charge multiplication ensues; these are the *secondary ionizations*. This is the key aspect where ICs differ from the many other types of gas-filled detectors because ICs function without charge multiplication.

An applied voltage vs. ionization current, sometimes called an *I-V Curve*, is displayed below in Figure 3 which illustrates the aforementioned principle. Initially, as the voltage, $V$, is increased from zero, one sees the measured current continually increase. This occurs because the electrons in the gas gain more and more energy to resist the various phenomena which can diminish the maximum signal (see Sec. 3.1.). After $V$ reaches some threshold voltage, these detrimental phenomena are overcome and saturation in the measured signal is achieved; this is the *saturation region* of an I-V curve and is where ICs operate. As $V$ continues to increase, the electrons gain enough energy to further ionize the gas molecules (*secondary ionizations)*, and one enters the various charge multiplication regions of an I-V curve.

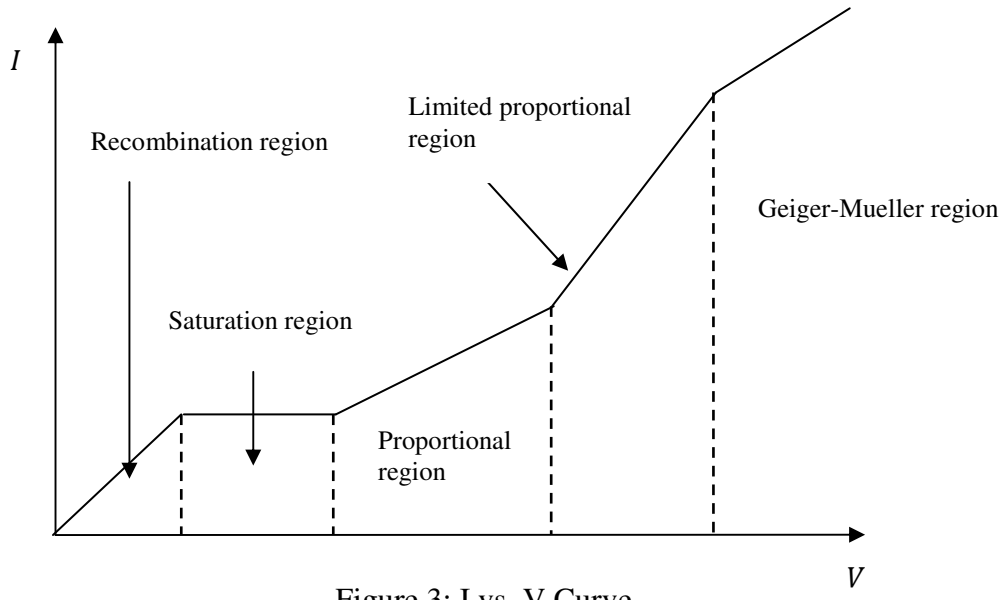



Figure 3: I vs. V Curve

Since ICs operate in the saturation region of Figure 3, the read-out signal is ideally constant over a wide range of voltages. One advantage of this aspect is that small fluctuations in the power supply should have no effect on the output signal (similarly electrical breakdown is less of a concern because of the lower applied voltages). Another advantage of ICs operating at lower voltages is since no charge multiplication occurring, the gas does not degrade as fast as it would in gases where charge multiplication is occurring; this increases the lifetime of the gas

### 2.3.4. Statistics of Ionization

The choice of fill gas used in an IC determines the geometry, voltages, and pressures that are usable for the detector along with our main parameter of interest, the energy resolution. As stated above, when an ionizing particle transverses the active region of the IC, it loses its energy by ionizing the gas molecules. The number of electron-ion pairs

formed is a function of the fill gas, the type of incident particle, and the particle's energy. On the other hand, the minimum energy to ionize an electron from an atom or molecule is simply the energy needed to break the electron bond; however some of the incident particle's energy also goes into excitations, vibrations, etc. of the gas molecules as well. With these two facts, to understand the ionization in a complex system, a parameter called the *W-value* is introduced and is defined as the average amount of energy lost by an ionizing particle per electron-ion pair formed. Typical *W*-values are on the order of 20-40 eV for most alpha and beta particles in gases of interest [Knoll].

If a charged particle is fully stopped within the active region of the IC then all of its energy is deposited in the gas. Therefore, the total *mean* number of electron-ion pairs formed, $n_0$, can be calculated with the *W*-value:

$$n_0 = \frac{E_0}{w} \qquad \text{Eq. 5}$$

where

$E_0$ = initial particle energy

$w$ = the average energy needed to produce an electron-ion pair

Precise measurements of the ionization process in gases show that the observed variance in $n_o$, ${\sigma_{n_0}}^2$, which, by Poisson statistics, is shown to be

$${\sigma_{n_0}}^2 = n_0 \qquad \text{Eq. 6}$$

is not in fact the true experimental variance. An empirical coefficient called the *Fano factor* is used to account for this phenomena. The Fano factor is simply defined as the observed variance in $n_o$ divided by the *Poisson-predicted* variance in $n_o$ and ranges from zero to unity. Typical Fano factors for the gases encountered in most gas-filled detectors range from about 0.05-0.20 [Knoll]. The Fano factor has direct implications on the energy resolution as will be shown in the following section.

### 2.3.5. Energy Resolution

One of the main properties of an IC, and the one of most importance to this work, is how well an IC can resolve the energy of an ionizing particle. This is quantitatively described by the *energy resolution* (ER) of the system, and for ICs it is defined by

$$ER \equiv \frac{FWHM(E_0)}{E_0} \qquad \text{Eq. 7}$$

where *FWHM* is the full width at half maximum of a signal produced by a particle having incident energy $E_0$. The *FWHM* can be shown to be [Knoll]:

$$FWHW = 2.35 * \sqrt{n_0 f} * w \qquad \text{Eq. 8}$$

where

$f$ = the Fano factor

$w$ = the average energy needed to produce an electron-ion pair

$n_0$ = average number of electron-ion pairs formed

Using the relation that for a Gaussian function, $FWHM = 2.35\sigma$, one can rewrite Eq. 7 to be

$$ER = \frac{2.35\sqrt{wf}}{\sqrt{E_0}} = \frac{2.35\sqrt{w}}{\sqrt{n_0}} \qquad \text{Eq. 9}$$

Eq. 9 represents the *minimum*, or best, ER obtainable by an IC due to just the statistical nature of ionization and does not take into account any other sources of uncertainty. For example, a 5.5 MeV alpha particle in P-10 gas, which is an argon-methane (90:10) mixture ($w$ and $f$ being 26.25 eV [Melton] and 0.18 [Masayuki] respectively), the best achievable ER is near 0.47%. This compares to a silicon surface barrier detectors with achievable resolutions as low as 0.1% for similar alpha particles [Knoll].

An IC very similar to our own, which analyzed 4.77 MeV alpha particles, got an ER just above 1.0% [Ammi]. Barrette et al. [Barrette] achieved an ER near 0.6% for 5.5 MeV alpha particles. Bertonlini [Bertonlini], who used a cooled-FET preamplifier, achieved an ER of 0.22% which was very close to his theoretical limit and also near that of which solid state detectors can attain in practice. These examples illustrate that the desired ER for our IC being less than 1.25% should be very realistic.

Eq. 7 and Eq. 9 show how the ER varies as $1/\sqrt{E_0}$, and therefore the best ER obtainable for fission fragments is about four times lower than that for alpha particles (assuming $w$ does not differ much between fission fragments and alpha particles, a good

approximation [ICRU]). This is the reason why the project's desired 1.25% ER for alpha particles may seem rather large at first, but because of this anticipated improvement from the statistics of ionization, the ER should improve when fission fragments are finally used. In practice, however, when using fission fragments the ER is generally limited by noise in the electronics simply because the statistics of ionization are much better with fission fragments and the electronic noise becomes the dominating factor. With that said, one should not hope for a factor of four better energy resolution as predicated when simply switching between alpha particles and fission fragments.

Koczon et al. [Koczon] obtained an uncertainty of 470 keV for their IC in a similar 2v-2E setup when using fission fragments (although it was not specified as to which fragment they were referring too). Another IC used at the Lohengrin Spectrometer obtained an ER of 0.6% for the light fission fragment [Bocquet]. A very similar IC to our own achieved ERs of 0.41 and 0.73% for the light and heavy fragment respectively [Oed].

### 2.4. Mass Resolution

If we combine the uncertainties in the previously mentioned time and energy measurements, not forgetting the uncertainly in the length, we arrive at the fractional uncertainty in the mass as shown above in Eq. 4. In relation to the fractional uncertainties in time and energy, the fractional uncertainty in the length, $\delta_l / l$, is generally very small and for all intents and purposes can be assumed to be zero. With that, Eq. 4 becomes

$$\frac{\delta_m}{\mathrm{m}} = \sqrt{\left(\frac{\delta_E}{\mathrm{E}}\right)^2 + \left(2\frac{\delta_t}{\mathrm{t}}\right)^2} \qquad \text{Eq. 10}$$

With a proposed time-of-flight distance of 62 cm, the respective $\frac{\delta_m}{\mathrm{m}}$ for the light and heavy fission fragments to achieve a *less than one amu resolution* are about 0.0045 and 0.0031 respectively. Using the $\delta_t$ are collaborators have reported for their time-of-flight measurement of 80 ps and the ER obtained by Oed et al. [Oed] as a starting point, the measured $\frac{\delta_m}{\mathrm{m}}$ would be 0.0041 and 0.004 respectively. The *less than one amu* goal is achieved for the light fragment yet not for the heavy fragment. Therefore, improvements are needed to the entire system to reduce $\delta_E$ or $\delta_\mathrm{t}$. Silicon-nitride windows are one main area where significant improvement should be achieved in the energy measurement (see Sec. 5.5), while the hopeful decrease in $\delta_t$ to 65 ps will be beneficial in the timing portion of the spectrometer.

Other experiments have used very comparable setups to analyze the mass of heavy ions, although generally with one arm and therefore with low intrinsic efficiency. Kozulin et al. [Kozulin] used a similar 2v-2E spectrometer, with surface barrier detectors in place of ionization chambers, and obtained a $\delta_m$ of about 1.7 amu for the elastic scatter of $^{48}$Ca off of $^{208}$Pb. Another 2v-2E setup, comprised of homemade START and STOP detectors, obtained a $\delta_m$ of 0.7 and 1.2 amu for the light and heavy fission fragment respectively [Koczon]. One of the main 2v-2E detectors currently being deployed, the Cosi-Fan-Tutte spectrometer, which has studied the thermal fission of $^{229}$Th, $^{239}$Pu, and $^{241}$Pu have obtained a $\delta_m$ around 0.6 -0.68 amu for the light fission fragment [Boucheneb, 1989;

Boucheneb, 1991; Schillebeeckx]. The heavy fragment, because of its poorer energy resolution (see Sec. 2.3.5), has not achieved a less than one amu resolution with the Cosi-Fan-Tutte spectrometer, nor to date with the best of our knowledge.

## 2.5. The Atomic Number Measurement

Recently ICs have been adapted to measure some of the characteristic properties of the Bragg curve of an ionizing particle [Gruhn]; this field has come to be known as *Bragg curve spectroscopy*. The Bragg curve is a measure of a particle's change in energy per unit distracted, $dE/dx$, as a function of the distance traveled (see Figure 4). The Bragg curve, for heavy charged particles, is described by the non-relativistic *Bethe-Bloche formula:*

$$\frac{-dE}{dx} = \frac{4\pi}{m_e c^2}\frac{nZ^2}{\beta^2}\left(\frac{e^2}{4\pi\varepsilon_0}\right)^2\left[ln\left(\frac{2m_e c^2\beta^2}{I(1-\beta^2)}\right) - \beta^2\right] \qquad \text{Eq. 11}$$

$m_e$ = rest mass of an electron

$n$ = electron density of the material

$Z$ = particle's charge

$c$ = speed of light in vacuum

$\beta$ = ratio of the particle's velocity to the speed of light

$e$ = elementary charge

$\varepsilon_0$ = vacuum permittivity

$I$ = mean excitation potential of the material

As a charged particle slows down within a material, its $dE/dx$ slowly increases for the majority of its range until an abrupt increase occurs in which the remaining amount of energy is lost. This sharp change near the end of a particle's path is called the *Bragg peak* and is a function of the particle's atomic number, *Z*. It should be noted that the Bragg peak is only seen in particles with energies greater than about 1 $MeV/amu$. A Bragg curve, in the context of ICs, can be thought of as the spatial distribution of electrons and positive ions formed along the path of the ionizing particle within the IC.

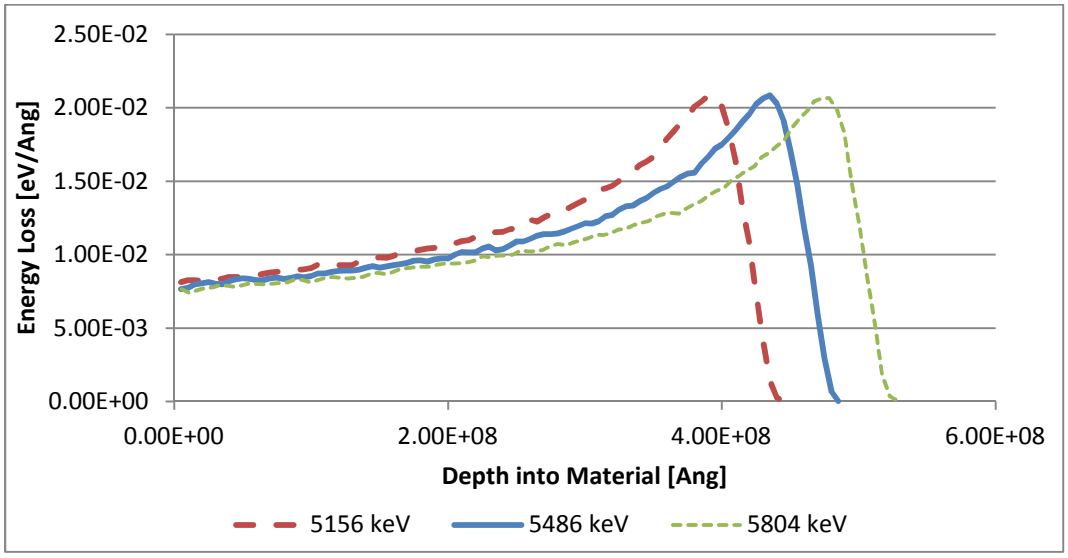



Figure 4: The Bragg curve for three different energy alpha particles as generated by SRIM

Figure 4 shows the Bragg curves for three alpha particles of different energies as generated from the *Stopping and Range of Ions in Matter* code, *SRIM* [Ziegler]. This simply shows the different ranges for different energy alpha particles, and the basic shape of the Bragg curve. More interestingly, if we overlap the same Bragg curves of Figure 4,

as in Figure 5, one sees how the Bragg peaks are very similar, indicating the similar $Z$-dependence of the three particles. On the other hand, Figure 6 shows how the Bragg peaks are substantially different for three different $Z$-particles, even though each have the same $MeV/amu$ value. That illustrates the foundational premise of Bragg curve spectroscopy that different Z-particles display different Bragg peak characteristics, and therefore if one can measure the Bragg peak one gets a measure of the particle's $Z$.

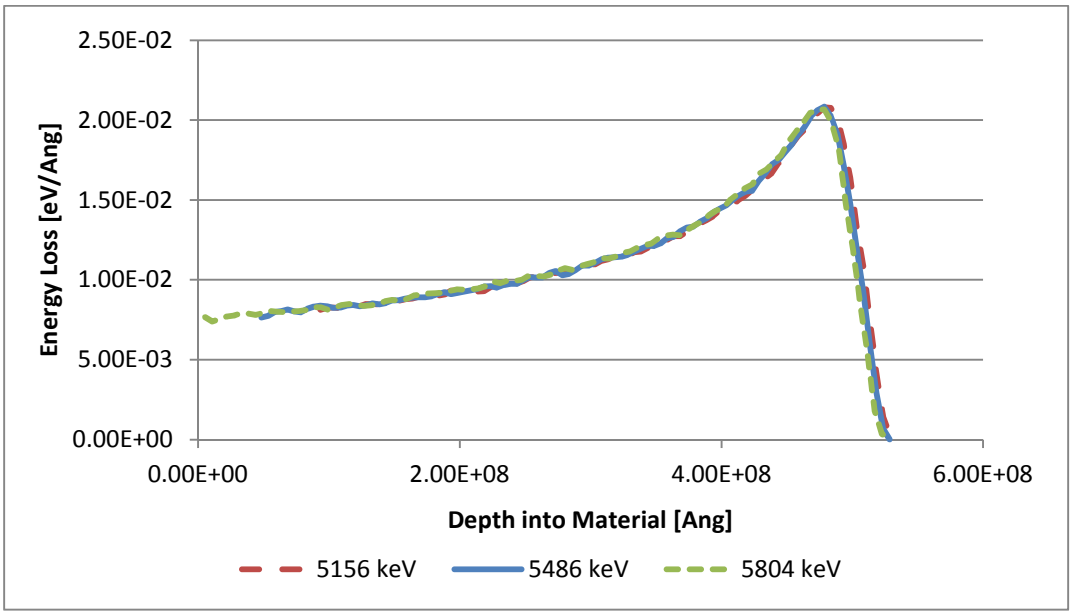



Figure 5: The Bragg curves from Figure 4 overlapped to show similar Bragg peaks as generated by SRIM

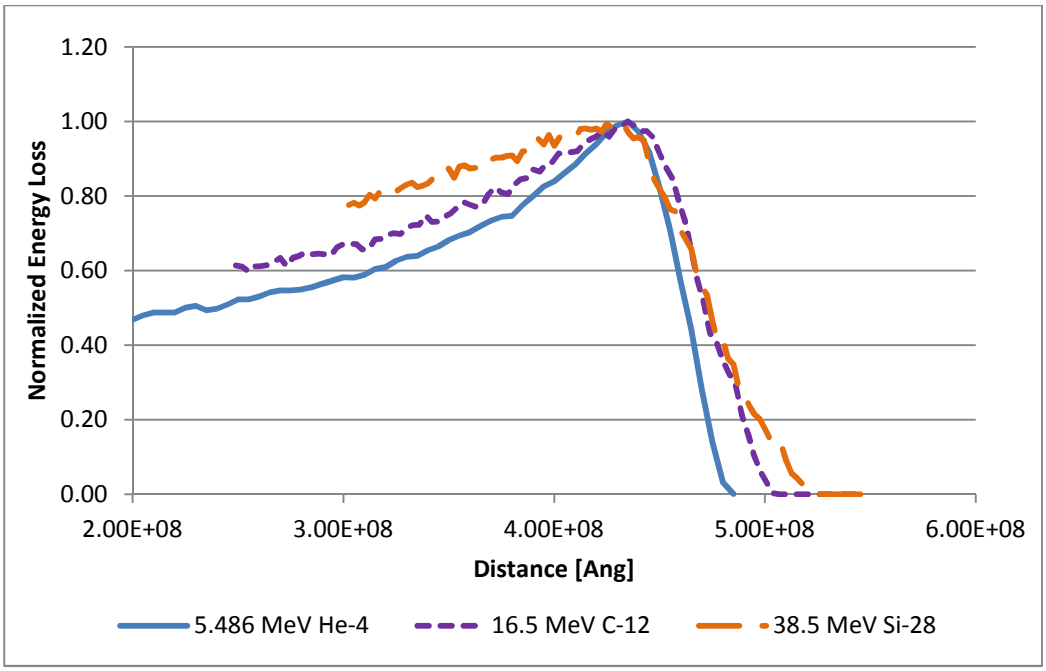



Figure 6: The normalized Bragg peaks for three particles with different atomic charges as generated by SRIM

The conventional way of measuring the Bragg peak involves using a linear amplifier with a short shaping time relative to the temporal width of the electrons within the IC [Gruhn]. The shaping time of a linear amplifier can be thought of as the time in which one is collecting a signal. If one wants to measure a full signal, then one needs to select a shaping time much larger than the temporal width of one's signal. On the other hand, if one wants to measure just the beginning portion of a signal, than a shaping time *less than the temporal width* of the signal is desired. Because the output signal from the anode of an IC is the a *time-reserve* image of the Bragg curve, one simply needs a small shaping time to measure just the beginning portion of the Bragg curve, i.e. the Bragg peak, in order to gain a measure of the particle's *Z* (See *Appendix A* provides a more in-depth look at the details of the signal processing used for Bragg curve spectroscopy). Because the

Bragg peak generally only occurs for particles with energies greater than 1 $MeV/amu$, a different approach is used for the lower energy particles like fission fragments.

Many groups, including Ochiishi et al. [Ochiishi; Sanami, 2009] have seen good results using the method mentioned above. In this technique, one varies the energy of a known $Z$-particle to get a figure similar to Figure 7, and then uses that data as a calibration plot for unknown $Z$–particles. Another approach employed by Sanami et al. [Sanami, 2008] use the drift time of the electrons in the chamber to indirectly measure the $Z$-dependent range of the ionizing particle, and with its energy and calibration plots, infer $Z$. This method has allowed them to successfully determine $Z$ at energies lower than 0.5 $MeV/amu$ as shown in Figure 7. This technique is the initial planned approach in measuring $Z$ for our spectrometer.

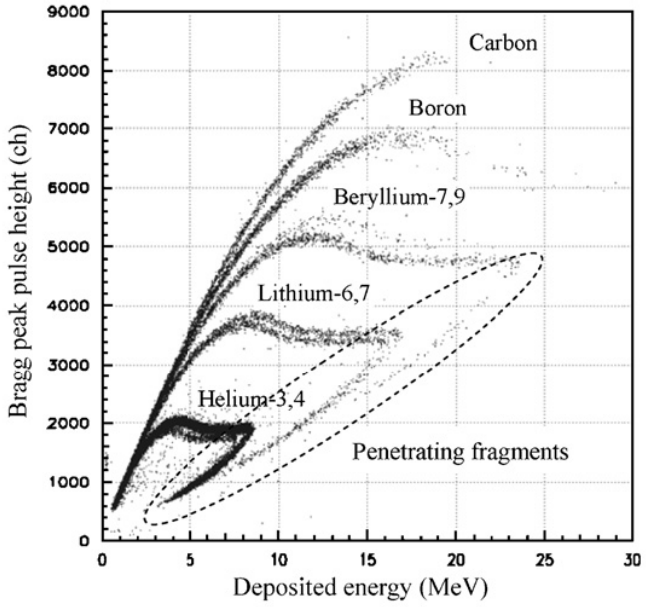



Figure 7: The Bragg peak vs. deposited energy for particles of different mass and atomic charge [Hagiwara]

## Chapter 3

## Detector Characteristics and Construction

---

### 3.1. Drift Velocity

As described above, the choice gas used is very important for the operation of any gas-filled detector. With respect to the operation of ICs, the most important parameter of the gas is called the *drift velocity.* The drift velocity is the terminal velocity electrons or ions obtain in a gas with an applied electric field due to the numerous collisions with gas molecules and the columbic force from the electric field. For electric field strengths found in most ICs, the drift velocity, *v,* for electrons and ions can be generally given as [Kapoor]

$$v = \mu_0 \frac{E}{P} \qquad \text{Eq. 12}$$

where

$\mu_0$ = the reduced mobility of the ion $[cm^2 * mbar/(V * s)]$

$E$ = electric field $[V/cm]$

$P$ = pressure $[mbar]$

Often times the parameter $E/P$ is grouped together and is known as the *reduced electric field*; it can be thought of as a force-over-resistance variable. The drift velocity is a rather important quantity when it comes to Bragg curve spectroscopy, where preserving the

spatial distribution in which the electrons are formed within the IC is essential. The drift velocity of electrons in P-10 gas is shown below in Figure 8.

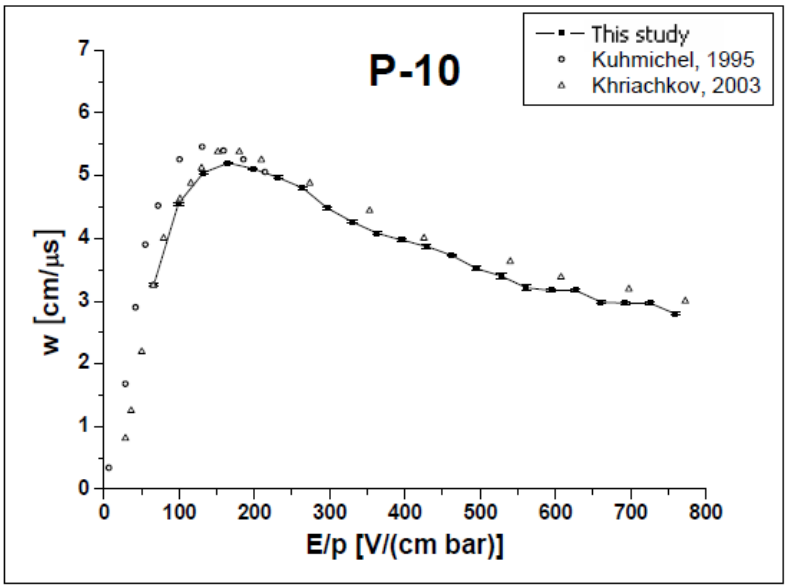



Figure 8: The drift velocity of electrons in P-10 gas [Göök, 2008]

To minimize the fill gas from capturing the signal electrons (see the following section), one wants to operate with the fastest drift time possible. So for example, when using P-10 gas, an $E/P$ value of near 150 $V/(cm * bar)$ should be selected. In this experiment, both the electric field and pressure were varied to quantify their affects on the operation of the IC, but in general the drift time of the electrons was around 1.8-2.3 µs based on Figure 8 and the spatial dimensions of our system.

### 3.2.1. Ion interactions

After a molecule of gas is ionized, there are a number of interactions by which the electron and positive ion may proceed by which can ultimately affect charge collection,

and therefore the measured signal. The following analysis is restricted to just the electrons as the signal carriers because the heavy ions are far too slow for most signal processing applications due to their much larger mass. The two main interactions electrons can encounter within the IC are electron capture and recombination. Along with these two, diffusion and space charge, which are intrinsic to all gas-filled detectors, can also limit the overall signal obtained by an IC.

### 3.2.2. Electron Capture

Electron capture, sometimes called as *charge transfer*, occurs when a neutral gas molecule acquires one of the signal electrons. Depending on the molecule which acquires the electron, this newly formed negative ion can be quite stable and the electron can be successfully removed from signal collection. For the classic two-body electron capture process, there are two main mechanisms in which an electron can be removed:

$$A + e^- \rightarrow A^- \qquad \text{Eq. 13}$$

and

$$A + e^- \rightarrow A^{*-} \rightarrow \mathrm{B}^- + \mathrm{C} \qquad \text{Eq. 14}$$

The first mechanism is simply electron capture while the second is called *associative attachment,* and the energy brought by the electron goes into breaking apart the newly excited molecule into two products, *B* and *C*. For most gases the probability of $A^{*-}$

splitting up increases with increasing electron energies [Blum]. Most fill gases are chosen to minimize electron capture, but because of the presence of impurities in any system, these mechanisms must be mentioned due to their adverse affects on signal collection. The main impurities encountered in most gas-filled detectors are molecules that are highly electronegative such as oxygen, water vapor, and halogens.

The removal of electrons by electron capture is generally a time-dependant function proportional to the initial amount of electrons present, $n_0$. The number of electrons remaining, *n*, after a certain amount of time, *t*, can generally be given as [Khryachkov]:

$$n(t) = n_0 \exp(-t/\tau) \qquad \text{Eq. 15}$$

where

$\tau$ = the mean electron lifetime in the detector

By this definition, one wants the electrons to be present within the system for as little a time as possible, i.e. posses a large drift velocity.

Ahmed gives an example of how a 1% contamination of air gives rise to a 13% electron loss when the electrons travel merely 5 mm in argon gas [Ahmed]. A qualitative experiment was performed on our IC to demonstrate the effects of electron capture by air when a valve was opened and closed to allow the admittance of a small amount air into the chamber. An approximate 30 mbar increase in pressure was seen where air now

comprised about 3% of the total molecules of gas within the chamber. The resulting signal decreased by about 33% indicating the rather deleterious effects air has on the operation of ICs.

Electron capture can be easily reduced by eliminating the presence of any electronegative gases in one's environment. Keeping a clean system, without leaks, and using a purified gas, in combination with a strong drift velocity seem to be the easiest and most beneficial ways in minimizing electron capture.

### 3.2.3. Recombination

When an electron and a *+1 ion* combine together to form a neutral gas molecule this process is called *recombination*, and as with electron capture the electron can be lost from signal collection. There are two general types of recombination: initial and volume.

Initial recombination (also known as columnar) occurs when an electron and positive ion from the *same* ionizing event combine together. With a higher ionization density this process is more common, so initial recombination is therefore proportional to the linear energy transfer (LET) of the ionizing particle and the gas pressure. High LET particles, like alpha particles and fission fragments, deposit their energy in very short distances increasing the likelihood of initial recombination simply because the charged particles are closer together. Similarly, higher gas pressures cause ionizing particles to stop at shorter distance, thus producing higher densities of electrons and positive ions. Volume recombination, on the other hand, occurs when an electron and a positive ion from

*unrelated* ionizing particles combine to form a neutral molecule and is therefore a function of the dose rate or activity of the ionizing radiation.

The very general equation of recombination [Knoll] looks at the time rate of chance of the concentrations of the position and negative ions:

$$\frac{dn^+}{dt} = \frac{dn^-}{dt} = \alpha n^+ n^- \qquad \text{Eq. 16}$$

where

$n^+$ = number density of positive ions

$t$ = time

$n^-$ = number density of negative ions

$\alpha$ = recombination coefficient

One can see in Table 1 that argon has a very small α, which is attributed to the *Ramsauer minimum* in its attachment cross section [Sauli]. On the other hand, hydrogen gas and air have significantly larger α values, due in part to their more complex bond structure; an electron interacting with one of these gases can lose substantially more energy due to larger inelastic cross sections, and therefore become more susceptible to recombination.

| Gas | $\alpha$ [cm$^3$/s] |
|---|---|
| He | $6.8 \times 10^{-9}$ |
| Ar | $6.8 \times 10^{-11}$ |
| Air | $1.7 \times 10^{-7}$ |
| $H_2$ | $1.6 \times 10^{-7}$ |

Table 1: The recombination coefficients for various gases at STP [Brown]

A more detailed theory of recombination was developed by J. J. Thomson. To understand his theory, consider two ions in the vicinity of each other. If one ion suffers a *thermalizing* collision with some external third body where it loses a sufficient amount energy *and* ends up within some critical distance from the other ion, these two ions will be bound together because the coulumbic attraction exceeds the total thermal energy of the system:

$$\frac{e^2}{r} > \frac{3}{2}kT \qquad \text{Eq. 17}$$

where

$e$ = the elementary charge

$r$ = the distance between the two particles

$k$ = the Boltzmann Constant

$T$ = absolute temperature

Thomson's theory of recombination works well for pressures above a few mbar but is limited above about 1300 mbar [Brown].

Besides selecting gases with small recombination coefficients, to minimize recombination one can also apply strong electric fields values, *E*, within the IC. Böhm [Böhm] shows how the losses due to initial and volume recombination in air-filled ICs at STP are proportional to$1/E$ *and* $1/E^2$ respectively. One can assume that the loses for other types of gas would follow a similar trend in that a larger electric field reduce these effects as well.

### 3.2.4. Diffusion

In addition to the processes described above, the electrons will also naturally diffuse through the gaseous medium by undergoing numerous collisions with the gas molecules, and as a result, there will be a tendency for the electrons to leave the IC. To grasp how the electrons are diffusing in the presence of an electric field, one can look at the standard deviation of their traveled path. An ion cloud traveling a distance *x* in a gas with an electric field and pressure dependent diffusion coefficient *D,* when characterized by a Gaussian distribution, will have a spatial distribution which can be described with a standard deviation, $\sigma_x$, [Sauli] of

$$\sigma_x = \sqrt{\frac{2Dx}{v}} \qquad \text{Eq. 18}$$

where

$v$ = the drift velocity of the particle

The energy of the drifting electrons can be substantially different depending on what type of gas they are in. In *cold gases*, the energy of the electrons won't deviate much from thermal energy even when large electric field values are applied, and therefore using the *Nernst-Townsend formula,*

$$\mu kT = eD \qquad \text{Eq. 19}$$

is a valid approximation (where $\mu$ is the ion mobility). With that approximation, Eq. 18 can be rewritten as

$$\sigma_x = \sqrt{\frac{2kTx}{eE}} \qquad \text{Eq. 20}$$

Eq. 20 represents the *thermal limit of diffusion* and is applicable to electrons drifting in cold gases. Diffusion becomes more of a concern when electrons are drifting in *hot gases,* where the average energy of the electrons can be significantly altered at increasing electric field values. In this case, a correction to Eq. 20 is needed based on the properties of the gases involved.

Another aspect of diffusion is its directionally with respect to the electric field. The diffusion of electrons in the direction parallel to the electric field (the longitudinal direction) and in the direction perpendicular to the electric field (the traverse direction) can be different depending on whether the collision frequency of the electrons with the gases molecules increases or decreases with electron energy. The reader is directed to

[Parker] or [Skullerud] for a good description of this phenomenon. In short though, when considering electrons diffusing as a cloud, the authors show how the mobilities of the electrons in the leading edge of the electron cloud differ from those at the trailing edge giving rise to different diffusion characteristics of the two regions. Therefore, the ratio of the diffusion in the longitudinal direction to the transverse direction can be greater or smaller than unity depending on the gas used.

### 3.2.5. Space Charge

Space charge, like diffusion, is a natural affect occurring in all gas-filled detectors and is simply the presence of coulombic charges in the detector. With respect to ICs, space charge can distort the detector's collecting electric field and thus create harmful effects on the functionality of the IC. As previously mentioned, the substantial mass difference between the electrons and positive ions means the electrons drift roughly 1000 times faster than ions, and for all intents and purposes, the positive ions can be considered stationary while the electrons drift. With that, the positive ions' charge will now distort the initially constant electric field (magnitude and or direction), which will in turn affect the electrons' motion through the detector.

Every ionization produces an electron-ion pair, and as a result every swarm of electrons traveling to the anode will experience a somewhat distorted electric field. One can assume that this distortion should be about the same every time and therefore every electron swarm is affected by approximately the same distorted electric field. If this is the case, space charge probably poses no problem for electron collection. However,

where the effects of space charge certainly become problematic is for high dose rates or activities. If the positive ions do not have enough time to drift to their respective electrode before another ionizing particle arrives, the field could be significantly distorted (not to mention the increased possibility of volume recombination), and therefore different electron swarms would feel different electric fields.

In our chamber, the maximum amount of time it would take the positive ions to drift to their electrode, and therefore be removed, would be about 0.002 s, whereas our highest activity was about 3.4 counts per second. In this situation, space charge was not a statistically significant concern.

### 3.2.6. Conclusions

All the effects described in Sec. 3.2. are detrimental to the operation of an IC and should be minimized to the best extent possible. In general though, if one operates with a clean detector environment, large spatial dimensions to limit diffusion, and an electric field strong enough so as to be operating in the saturation region of Figure 3, these effects will become insignificant in most applications.

## 3.3. The Ionization Chamber Pulse Height

To gain useful information from an IC, one needs to electronically wire it appropriately so as to gain a measure of the energy of an ionizing particle. An IC can be operated in either pulse mode of current mode (See Appendix B), and the following will be restricted to pulse mode because it is commonly how ICs are operated when energy and timing

information is desired. Generally an IC measures a voltage across a resistor of resistance *R*, where a virtual capacitor of capacitance *C* represents the stray capacitance across the detector and from the various cables used as indicated in Figure 9. The active charge collection region of the IC is located between the cathode and anode, where *x* represents an example location of an electron-ion pair.

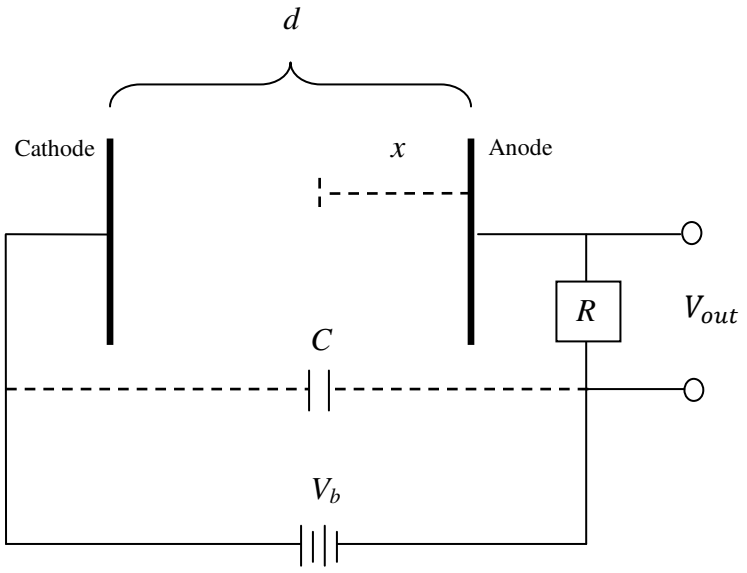



Figure 9: The basic circuitry used to measure a voltage from an IC when it is operated in pulse mode

The readout signal, $V_{out}$, is not produced from charge collection, but rather from energy changes in the system due to the motion of charge particles in an electric field. For the following derivation [Ahmed], one assumes the IC to be infinitely long. We first define

$$V_{out} \equiv V_b - V_{\mathrm{em}}(t) \qquad \text{Eq. 21}$$

where

$V_b$ = the supplied bias

$V_{\mathrm{em}}(t)$ = the voltage caused by the movement of charged particles

t = time in which the electromagnetic charged particles are moving

Keeping in mind that an IC is just a capacitor, the energy, *U*, stored in an a IC of capacitance, *C,* with a voltage, *V,* across its conductors is given by the general equation

$$U = \frac{1}{2}CV^2 \qquad \text{Eq. 22}$$

The energy, T, taken away from the system by the movement of a number of charged particles is

$$T = n_0 q E v t \qquad \text{Eq. 23}$$

where

$n_0$ = the number of charged particles

q = the charge of the particle

$E$ = the electric field

$v$ = the velocity of the charged particles

$t$ = the time spent in the IC

With conservation of energy before the charged particles are liberated from ionization and during the movement of the particles, one arrives at the following equation:

$$\frac{1}{2} C {V_b}^2 = n_0 q E v_+ t + n_0 q E v_- t + \frac{1}{2} C {V_{em}}^2 \qquad \text{Eq. 24}$$

where

$v_+$ = the velocity of the positive ions

$v_-$ = the velocity of the negative ions

Eq. 24 can be rearranged to be

$$\frac{1}{2} C \left({V_b}^2 - {V_{em}}^2\right) = n_0 q E t (v_+ + v_-) \qquad \text{Eq. 25}$$

and then finally into

$$\frac{1}{2}C(V_b - V_{em})(V_b + V_{em}) = n_0 q \frac{V_b}{d} t(v_+ + v_-) \quad \text{Eq. 26}$$

With the knowledge that $V_{out}$ is very small, Eq. 21 can be approximated as

$$V_{em} \cong V_b \quad \text{Eq. 27}$$

With that, Eq. 26 now becomes

$$\frac{1}{2}CV_{out}2V_b = n_0 q \frac{V_b}{d} t(v_+ + v_-) \quad \text{Eq. 28}$$

which can finally be rearranged into Eq. 29 which represents the output voltage caused by the drift of both the positive and negative ions.

$$V_{out} = \frac{n_0 q}{Cd} t(v_+ + v_-) \quad \text{Eq. 29}$$

If the negative ions are born at a distance *x* from the anode (see Figure 9), then the positive ions are born at a distance *d-x* from the cathode. Likewise, their traveled distances can be represented as $x = v_- t_-$ and $d - x = v_+ t_+$ respectively (where $t_-$ and $t_+$ are the drift times of the negative and positive ions respectively). With that, and the knowledge that the electrons travel much faster than the positive ions so that the motion of the positive ions can be considered negligible when the negative ions are drifting, one

arrives at the piecewise equation for $V_{out}$ as a function of time which is also graphically illustrated in Figure 10:

$$\begin{aligned} \frac{n_0 q}{Cd} t(v_+ + v_-) \quad &: \quad 0 \le t \le t_- \\ \frac{n_0 q}{Cd} t(v_+ + x) \quad &: \quad t_- \le t \le t_+ \\ \frac{n_0 q}{C} \quad &: \quad t_+ \le t \end{aligned} \qquad \text{Eq. 30}$$

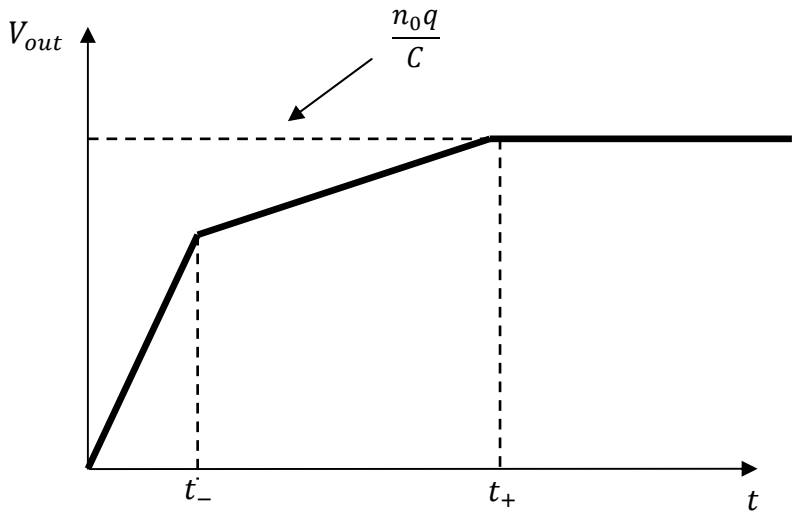



Figure 10: The output voltage as a function of time in an IC when both the voltages caused by the positive and negative ions are measured [Ahmed]

When looking at Figure 10, one sees an initial steep rise in $V_{out}$ caused by the fast drift of the electrons up to $t_-$ (in this region the slow drift of the positive ions provides a negligible contribution to the entire signal). This is followed by a more gradual rise in $V_{out}$ during which only the slower positive ions are drifting. After all the positive ions

are collected, the maximum $V_{out}$ is obtained. This initial, fast rise caused by the electrons is very advantageous in signal processing due to the fact that one wants to collect the signal very quickly as to eliminate dead time, electron capture, etc.

This over simplistic approach shows how an IC can be used to measure a voltage and relate it to $n_0$, which is in turn proportional to the energy of an ionizing particle based on Eq. 5. Two problems arise from operating an IC in this fashion. The first is that the positive ions' drift time is considerably larger than that of the electrons and thus not suitable for most applications. The second is if one can in fact remove the positive ions' contribution to $V_{out}$, Eq. 29 becomes

$$V_{out} = \frac{n_0 q}{Cd} x \qquad \text{Eq. 31}$$

In this case, $V_{out}$ is now proportional to the distance where the electrons were born and is not ideal. A technique designed to eliminate both of these effects uses a screening electrode called a *Frisch grid*.

### 3.4.1. The Frisch-gridded Ionization Chamber Pulse Height

A Frisch-gridded ionization chamber employs a gridded electrode located between the cathode and anode to screen the anode from the induced charges produced by the drift of the negative and positive ions in the cathode-Frisch grid region of the detector; it also removes the positional dependence on $V_{out}$. Figure 11 shows the geometry of a Frisch-gridded ionization chamber and circuitry used to measure $V_{out}$ (where *A* is the distance

between anode and Frisch grid, *B* is the distance between Frisch grid and cathode, *d* is the distance from the center of one wire to the other, and *r* is the radius of each wire comprising the Frisch grid). In this case, a signal is only produced on the anode once a charged particle (in this case an electron) crosses the Frisch grid. Now the measured signal is caused solely by the electrons with this mode of operation being called *electron sensitive mode*. Also, because the anode only *sees* the electrons once they cross the Frisch grid, it removes the positional dependence on $V_{out}$ because now, to the anode, it appears as though all the electrons travel the same distance *A* within the chamber.

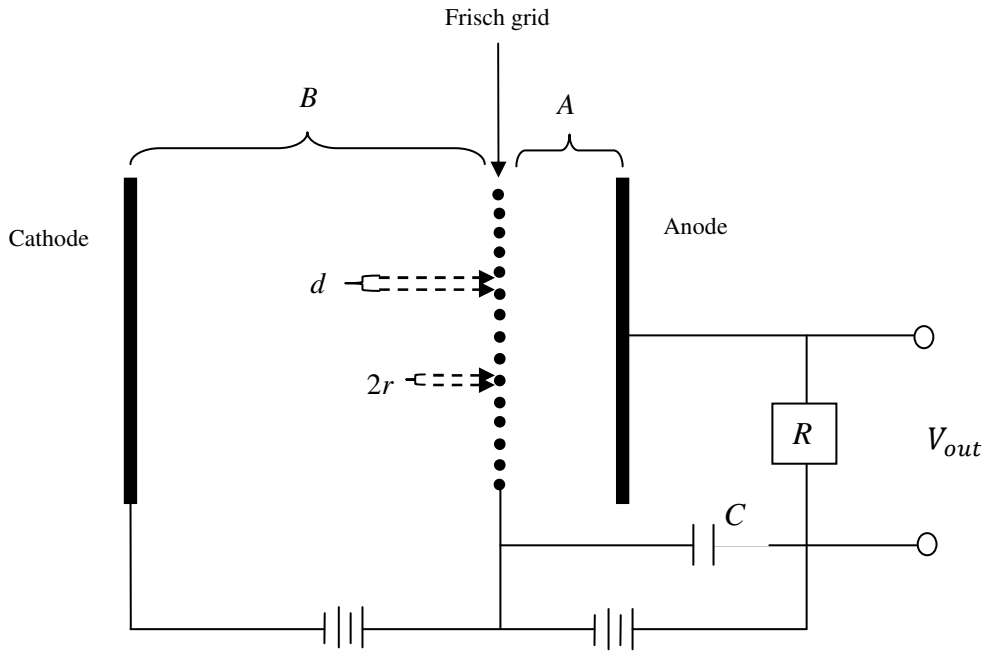



Figure 11: The basic geometrical and electric layout of a Frisch-gridded IC

Because a Frisch-gridded IC screens the voltages induced by the positive ions, it therefore removes the positive ions contribution to $V_{out}$, and now Eq. 30 and Figure 10 are replaced by Eq. 32 and Figure 12

$$\begin{aligned} 0 \quad &: \quad 0 \le t \le t_{1-} \\ \frac{n_0 q}{Cd} v_t \quad &: \quad t_{1-} \le t \le t_{2-} \\ \frac{n_0 q}{C} \quad &: \quad t_{2-} \le t \end{aligned} \qquad \text{Eq. 32}$$

where

$t_{1-}$ = time it takes the electrons to reach Frisch grid

$t_{2-}$ = time it takes the electrons to reach anode

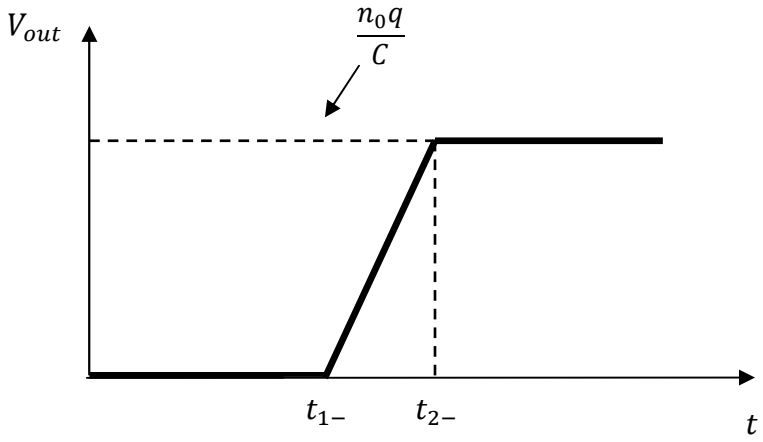



Figure 12: The output voltage as a function of time in a Frisch-gridded IC where only the voltages from the negative ions are being measured [Ahmed]

### 3.4.2. Frisch Grid

The Frisch grid, being a grid rather than a continuous membrane, does not completely shield the anode from the drift of the charges in the cathode-Frisch grid region and therefore some voltage will still be induced on the anode. Bunemann [Bunemann] investigates this shielding effect of the Frisch grid and creates the parameter, $\sigma$, which denotes the grid's *inefficiency* of screening out an induced voltage from the drift of charged particles in the cathode-Frisch grid region from the detector. The derivation of $\sigma$ assumes the Frisch grid is made of just parallel wires and that $d$ is much smaller than $A$. With that, $\sigma$, is approximated to be

$$\sigma \approx \frac{d}{2\pi A} \log\left(\frac{d}{2\pi r}\right) \qquad \text{Eq. 33}$$

One sees in Eq. 33 that by increasing the Frisch grid-anode distance, increasing the radius of the wire, or decreasing the pitch of the grid; the Frisch grid acts as a better shield for the anode (one is directed to [Bunemann] to see why one cannot simply set $d = 2\pi r$). In our experiment, because we were using a Frisch grid with parallel and perpendicular wires, we could not use Eq. 33 to approximate $\sigma$. However, if it had been made of just parallel wires, σ would have been less than 2.5%.

Since σ can never completely be zero, some of the moving charge from the cathode-Frisch grid region will always induce a voltage on the anode before any electrons have crossed the Frisch grid. Göök et al. [Göök, 2012], along with Al-Adili et al. [Al-Adili], use the Shockely-Ramo theory and experiment to better quantify this phenomena and

conclude that an additional rise in the anode signal, proportional to $\sigma$, is seen but is generally very small.

Another concern arising from the use of a Frisch grid is that the grid still must be transparent to the electrons. Because the Frisch grid is biased to some intermediate voltage relative to the cathode and anode, there will be some tendency for the lines of force, i.e. the electric field lines in which the electrons travel "on," to terminate on the grid wires. Bunemann [Bunemann] goes on to derive the following condition, which if satisfied, states that all field lines will pass through the Frisch grid and terminate on the anode:

$$\frac{E_{FG-A}}{E_{C-FG}} \geq \frac{1+\frac{2\pi r}{A}}{1-\frac{2\pi r}{A}} \qquad \text{Eq. 34}$$

where

$E_{FG-A}$ = the electric field between the Frisch grid and anode

$E_{C-FG}$ = the electric field between the cathode and Frisch grid

This condition is obviously very desirable to achieve and Frisch-gridded ICs should always satisfy it. The ratio of the electric fields in the two regions, for the majority of this experiment, was set to 2.8 and the above condition was sufficiently satisfied. This parameter was also varied in Sec. 4.8.

### 3.5.1. Detector Construction and Components

The Frisch-gridded IC designed for this experiment, shown in Figure 13, was of axial geometry, and the design by Oed et al. [Oed] was used as a general guideline. Figure 14 shows a cross sectional view of the IC; its major components are discussed below.

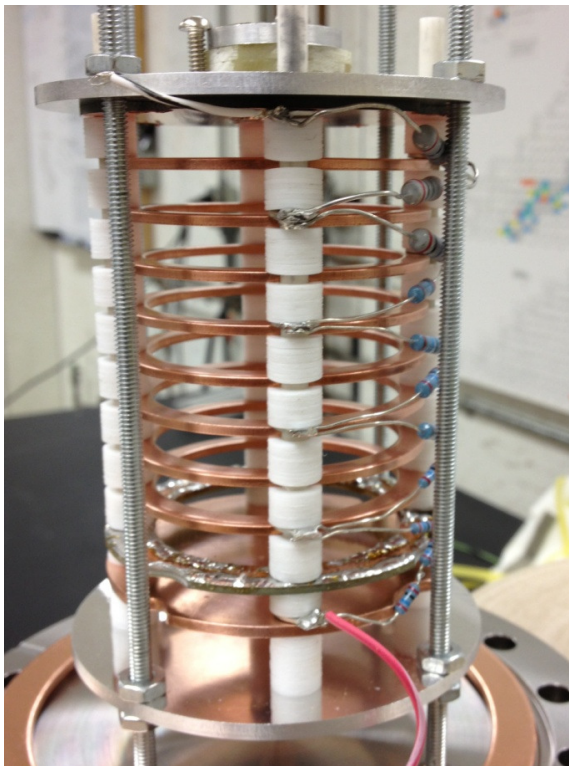


Figure 13: The IC designed and built for the various experiments

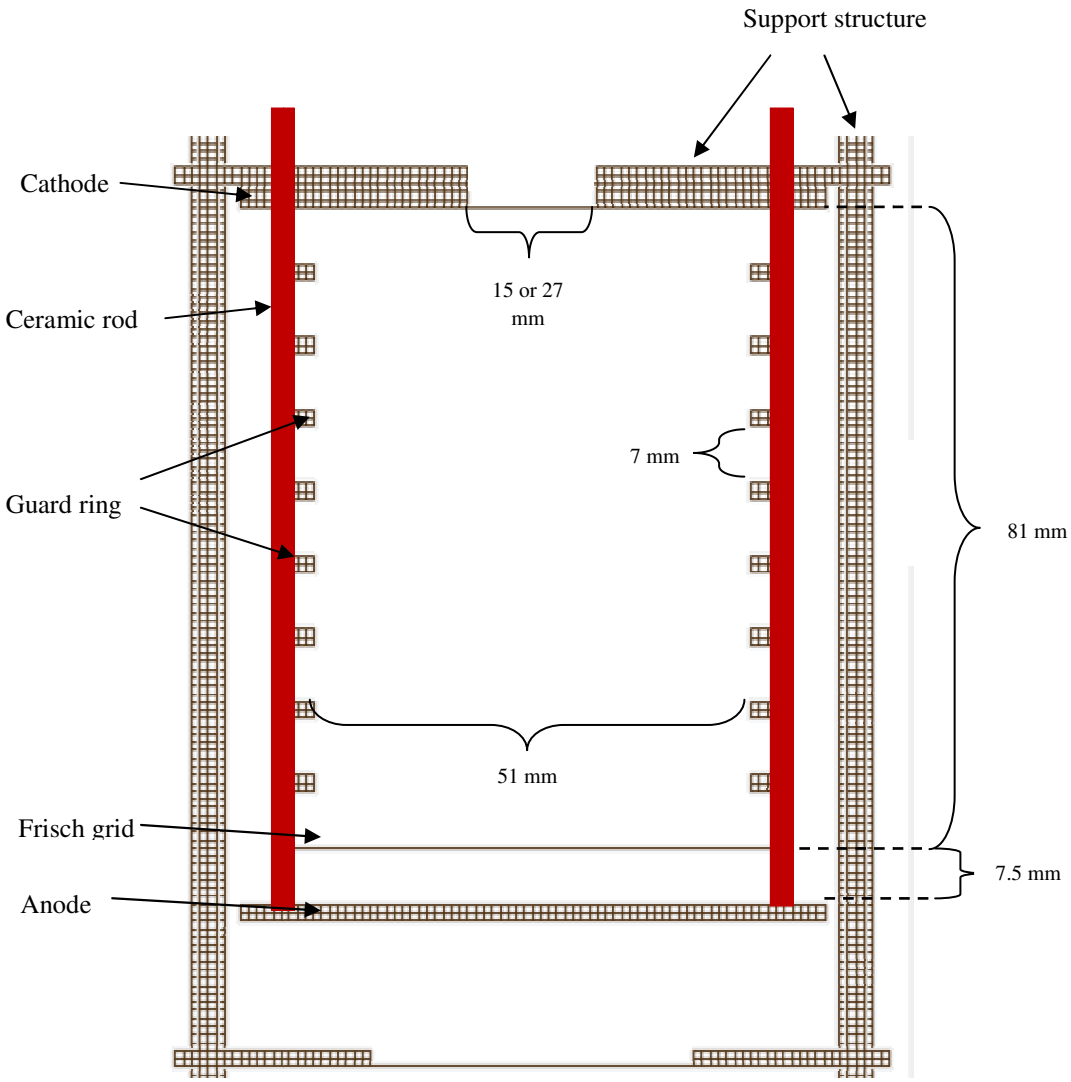



Figure 14: A cross-sectional view of the IC where ionizing particles from the top

At the top of Figure 13 is the cathode. It is made of one-side, copper-plated Fr4 circuit board, where the plated side points toward to anode to establish the electric field. The cathode was set to ground potential and tied-off to the chamber. The cathode also doubles as the entrance of the IC where its opening is partially covered with a small, eight-wire grid. This *cathode grid* (see Figure 15) was made of 25 µm diameter gold-

plated tungsten wires spaced one mm apart and soldered to the cathode. Without the cathode grid, the electric field would be significantly distorted and it is therefore a necessity to obtain a very homogeneous electric field within the IC. Careful consideration was taken to minimize the amount of solder used simply because large amounts of solder would give rise to additional distortions in the electric field (not to mention an increase in outgassing of deleterious gases). The geometrical transmission of the cathode grid for alpha particles was calculated to be greater than 97%.

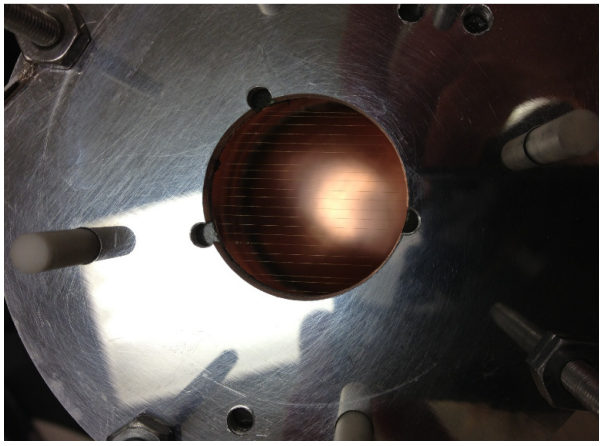


Figure 15: The top of the IC showing the cathode grid and support structure

The eight copper guard rings (whose purpose is described below in Sec. 3.6) were each separated by nine Teflon spacers and ultimately held in place by four ceramic rods. The use of Teflon and ceramic were chose because of their superb insulation properties along with ceramic's good resistance to radiation damage [Knoll]. All electrical components were biased successively by a resistor chain of eleven resistors (~220 MΩ total). The change in voltage between successive guard rings, which should be constant, had fluctuates of less than ±3% due to the uncertainty in the resistor values.

The Frisch grid (Figure 16) is made of the same material and dimensions as the cathode grid. It is in the crossed-wire configuration, which has been shown to possess a smaller σ [Göök, 2012]. The Frisch grid holder, which is what the Frisch grid is actually soldered onto, was made of Fr4 circuit board like the cathode. Finally, the anode is simply a copper disk and is where the signal is actually extracted from.

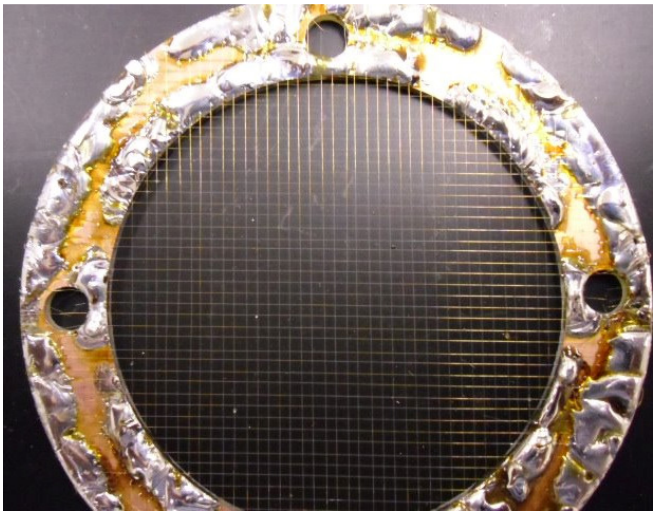


Figure 16: The mesh Frisch grid built for the various experiments

The distance from cathode to Frisch grid was based on the desired operational pressures and the ionizing particles' corresponding range in P-10 gas. This distance was set to about 81 mm and allowed us to comfortably operate at pressures as low as 575 mbar for alpha particles, and therefore significantly lower for fission fragments because of their shorter stopping distance (~150 mbar). The distance from Frisch grid to anode was chosen to be 7.5 mm to satisfy Eq. 34, yet also to keep σ small (Eq. 33).

The IC is held within a large stainless steel beam pipe (see Figure 17 and Figure 18) that is completely filled with gas during operation. The two ends of the beam pipe were closed-off with flanges, one containing the high-voltage/signal feedthrough and gas-in supply ports, while the other contained the vacuum pump and pressure gauge ports. The former flange also contained the IC itself, which was threaded into the flange by metal rods. These metal threaded rods form the backbone of the support structure which keeps the IC in place. The Kurt J. Lesker Company bourdon style pressure gauge used works well for pressures in the range of 1-1300 mbar and has a ± 2% on its pressure reading. A Teflon source holder, which also acts as a collimator (Figure 19), was used to ensure all alpha particle trajectories are kept within the active region of the IC.

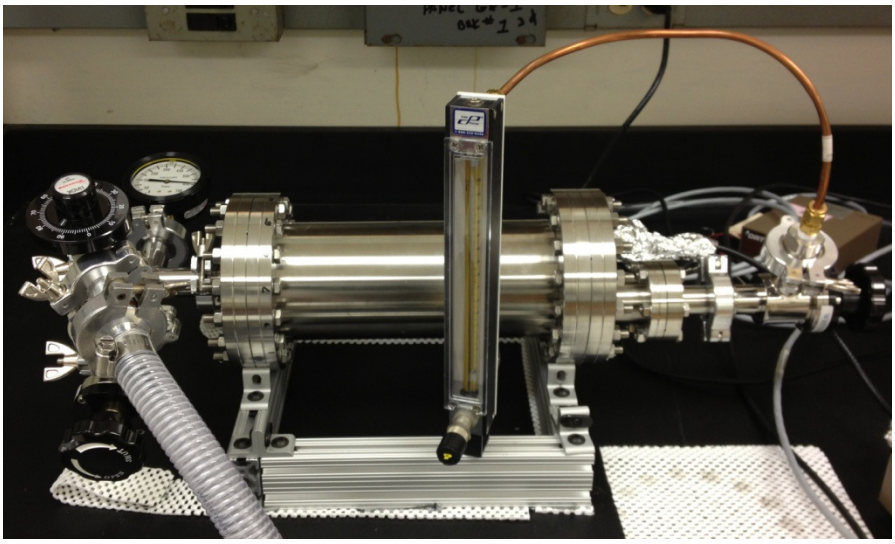


Figure 17: The external system used to house the IC

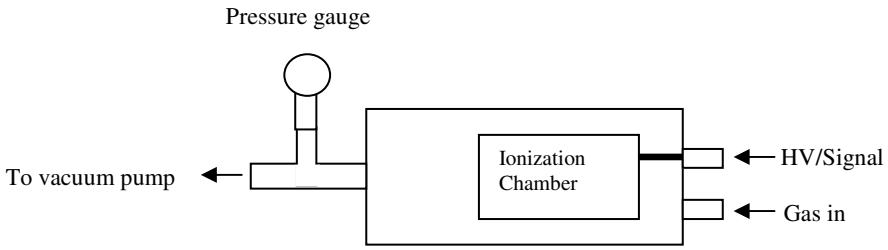



Figure 18: The external system used to operate the IC

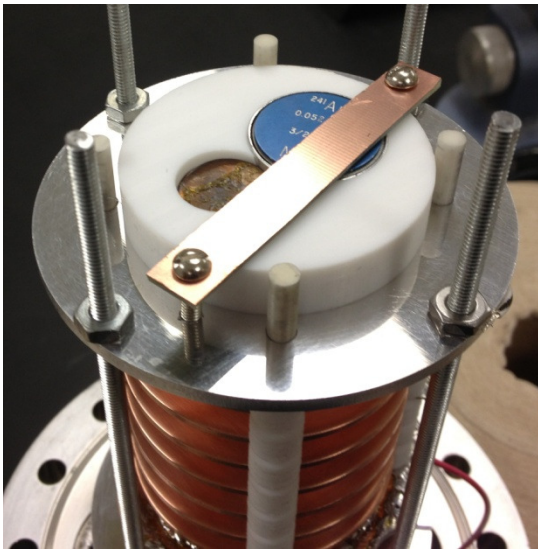


Figure 19: Top down view of the IC showing one of the collimator/source set-ups used

### 3.5.2. Noise

Along with the statistics of ionization (see Sec. 2.3.5), the other common source contributing to poorer energy resolution in ICs is electronic noise. Any electronic noise will add to the measured signal, shifting it from its true value, and as a result broadening the signal and therefore worsening the energy resolution. Radiofrequencies are a very common source of noise pickup in detectors, and one common way to combat this is by using short cables to reduce the length available to physically pickup this electromagnetic radiation. In our case, the signal wire connected from the anode to the SHV-feedthrough

within the chamber was made as short as possible to minimize this effect (see Figure 20). Also, not only do short cables reduce radiofrequency pickup, they also decrease the input capacitance as seen by the preamplifier.

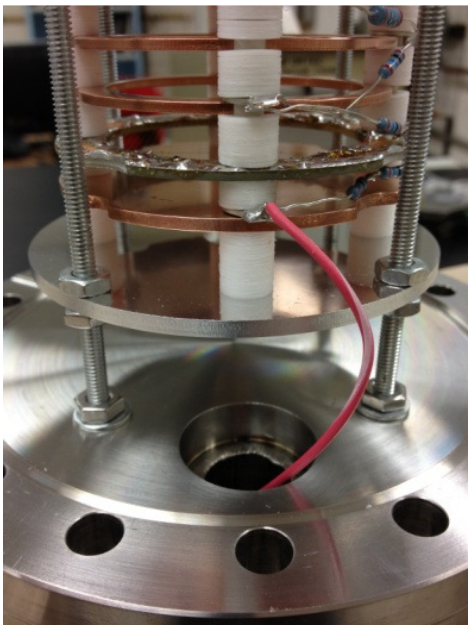


Figure 20: The signal cable

The input capacitance is defined as all the capacitance connected from the detector to the input of the preamplifier. The noise generated by a preamplifier increases with increasing input capacitance [Knoll], and therefore the minimization of it is desired. For ICs, the two main sources of input capacitance are the detector itself and the cabling used between the detector and preamplifier. The former is obviously tougher to change because it would involve altering the dimensions of the detector itself, but the latter can be minimized by using shorter cables. In our experiment a one ft long RG-59 cable connecting the detector to the preamplifier was always used. In an attempt to minimize input capacitance, we eliminated the cable altogether by making a modification to a

preamplifier so as to hook it up directly to the beampipe which houses the detector (Figure 21). This change lessened some periodic noise seen by the digital electronics, but the overall change in energy resolution in both the analog and digital systems was negligible.

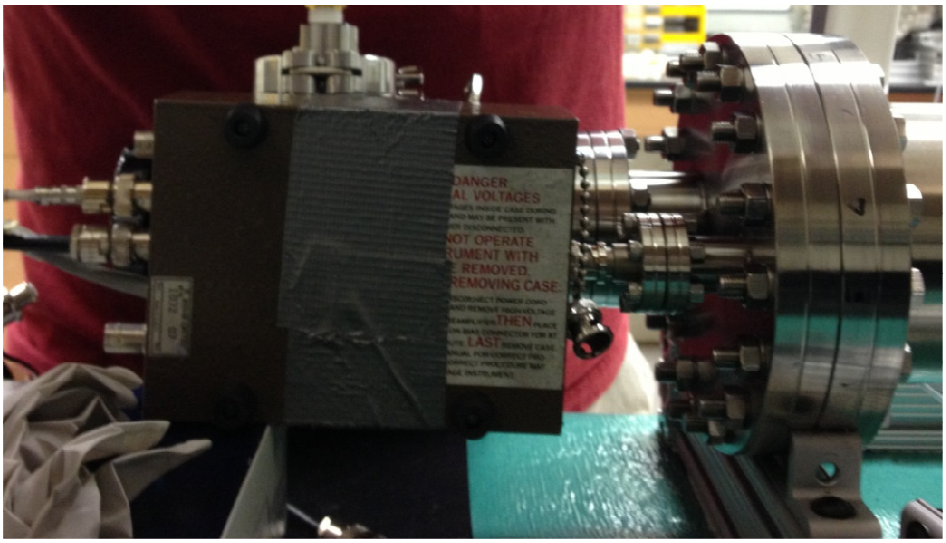


Figure 21: The preamplifier directly hooked-up to the beampipe which houses the IC

### 3.6. Guard Rings

One important feature common to most ICs is the use of *guard electrodes*, or guard rings. Guard rings are conducting rings placed around the active region of an IC, and whose purpose it is to maintain a constant electric field within the IC. A homogenous electric field is desired so that all electrons drifting in the IC will not be forced in odd directions, possibly out of the IC all together. Also in Bragg curve spectroscopy, where preserving the spatial distribution of the electrons is desired, a constant force, magnitude and direction, is needed so the relative positions of the electrons is maintained.

The guard rings are biased to some intermediate voltages relative to the cathode and Frisch grid, depending on the geometry used. For example, in our case because the guard rings are equally spaced, the voltage drop between successive guard rings is designed to be constant. Sec. 3.7.3 simulates different guard ring setups and their effects on the electric field's homogeneity. Guard rings also serve to limit leakage current between the cathode and anode [Knoll], which can add small fluctuations to a measured signal and is thus undesirable.

### 3.7.1. SIMION 8.1

The charged particle transport and electric field simulator code *SIMION 8.1* was used to simulate and analyze the electric fields within the IC. This program provided the grounds for selecting the distances and number of guards rings used to create a sufficiently homogeneous electric field

### 3.7.2 Electric Field

Figure 22 shows the electric field lines within the IC as generated by SIMION 8.1. There are two things to note about this design. First, the diameter of the anode and cathode are set larger than the diameter of the guard rings. This is done to minimize the field-bowing effects of the IC from occurring within the detector's active region. Second, the field lines tend to converge as one gets closer to the anode, signifying a change in direction of a particle's trajectories in this region. This affect is due to the proximity of the Frisch grid and anode, which are at relatively high voltage, to the grounded metal threaded support rods. This *focusing effect* is advantageous for electron

collection but not in Bragg curve spectroscopy, and therefore the metal threaded rods should be replaced with plastic rods to eliminate this effect during Bragg curve spectroscopy.

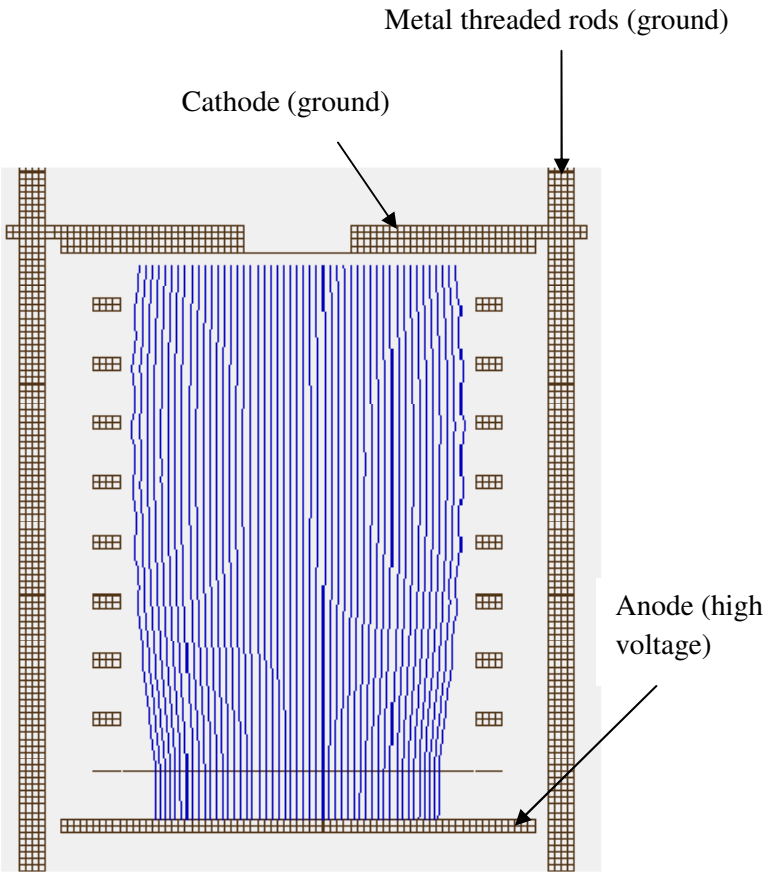



Figure 22: The electric field lines as shown in the middle of the IC

As mentioned above, the guard rings are used to establish a homogenous field within the IC. This is important for preserving the spatial distribution of electrons for Bragg curve spectroscopy and also to ensure that none of the signal electrons are leaving the chamber by odd electric field lines. The *guard ring technique* it is not perfect, and as a consequence the field within the IC does exhibit some heterogeneity. Figure 23 and

Figure 24 show a cross sectional view of the IC looking at the ratios of the simulated electric field at a point to the *analytical electric field* of the chamber in the cathode-Frisch grid and Frisch grid-anode regions respectively (the *analytic electric field* is defined as the constant electric field formed by an infinitely long parallel-plate capacitor of the same separation distance and voltage used for the IC). In Figure 23 the Frisch grid is located at 81 mm on the *Distance from Cathode* axis and the guard rings are located at ± 26 mm *Distance from Center* axis, i.e., the inner radius of a guard ring is 26 mm.

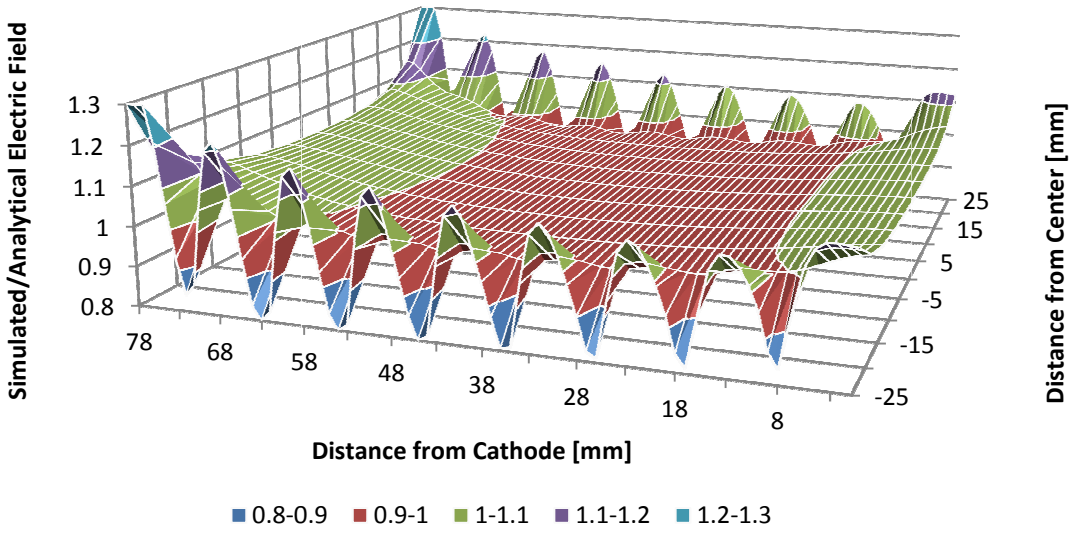



Figure 23: The ratio between the simulated and analytical electric fields in the cathode-Frisch grid region

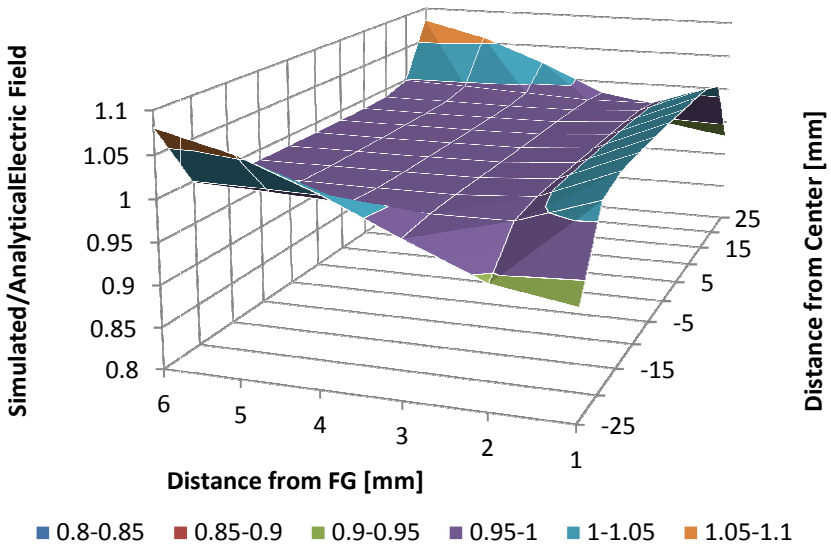



Figure 24: The ratio between the simulated and analytical electric fields in the Frisch grid-anode region

When looking at Figure 23 and Figure 24 one tends to see the simulated electric field deviate from the analytical field as one moves closer to any of the various electrodes comprising the IC. This explains the periodic and poor behavior of the ratio occurring near the edges of the IC due to the presence of the guard rings. On the other hand, the field is quite homogenous if one stays in the middle of the IC: the simulated value is generally inside 5% of its theoretical value if one is within a *distance from middle* being less than ±20 mm (this deviates when one is near the Frisch grid or cathode). A collimator was used in this experiment to ensure the alpha particle stayed within this bound.

### 3.7.3. Number of Guard Rings

A detailed simulated analysis on the homogeneity of the electric field within the IC was performed with SIMION 8.1 by varying the number of guard rings used but also keeping the cathode-Frisch grid distance as similar as possible (obviously if one inserts more guard rings and keeps the spacing between subsequent guard rings constant, the cathode-Frisch grid distance will be somewhat altered). Four different geometries of practical significance were simulated having the number of guard rings vary from eight to ten while the cathode-Frisch grid distance ranged from 79 to 86 mm. A parameter λ, which describes the geometry of the guard rings in relation to the overall length of the IC, is defined as

$$\lambda \equiv \frac{N}{d_{C-FG}} \qquad \text{Eq. 35}$$

where

$N$ = the number of guard rings in the cathode-Frisch grid region

$d_{C-FG}$ = the distance from cathode to Frisch grid

Through the analysis, a smaller λ shows a more homogeneous field near the middle of the IC, whereas a larger λ shows more homogeneity near the edge of the IC, i.e., near the guard rings. In the end though, the difference between the four setups was negligible, and a design of eight guard rings with a cathode-Frisch grid distance of 81 mm was chosen.

# Chapter 4

# Experiment and Results

---

## 4.1. Experiment Introduction

We performed various experiments to characterize and understand our ionization chamber (IC) with particular interest in the gas flow, lateral acceptance of the IC, shaping time of the linear amplifier, electric field, and gas pressure. Alpha particles were used to characterize these parameters.

## 4.2. Experimental System

Before any of the experiments were performed, the IC was always cleaned with ethanol and pumped down to sufficient vacuum (< 0.01 mbar) by an *Edwards XDS 10* vacuum pump. The fill gas used, P-10, which is an argon-methane mixture (90:10), was then slowly introduced into the system to the desired pressure.

As stated above, the initial testing of the IC was done with alpha particles as opposed to fission fragments due to their availability. The source used for the majority of the experiments was a tri-nuclide alpha source comprised of Pu-239, Am-241, and Cm-244. The main alpha energies of each nuclide are shown in Table 2. Each nuclide has multiple alpha energies, some of them very close to the others, but the energy resolution measured by a surface barrier detector for the 5486 keV peak in Am-241 was found to be less than 0.15%. This is sufficiently low enough so as to say the source itself (with its nickel-plate) or the intrinsic characteristics of the radionuclides should not significantly affect

the energy resolution as measured by our IC. The source had a very low count rate where statistically significant data took roughly a day to gather. A change was made to use a higher activity Pu-239 source in combination with a different Am-241 to decrease the count time so as to allow us to characterize our system in much shorter times.

| **Pu-239** | | **Am-241** | | **Cm-244** | |
|---|---|---|---|---|---|
| Energy | Branching | Energy | Branching | Energy | Branching |
| 5106 | 11.94 | 5443 | 13.1 | 5664 | 0.02 |
| 5144 | 17.11 | 5486 | 84.8 | 5763 | 23.1 |
| 5157 | 70.77 | 5545 | 0.37 | 5805 | 76.9 |

Table 2: The sources used for the experiment, where energies are given in keV and branchings in percentages [Brookhaven National Laboratory]

The readout system used is shown below in Figure 25 (the thicker lines represent the biasing of the various components). The preamplifier used was an Ortec 142 PC charge sensitive preamplifier. The 142 PC has very low noise with the RMS number of electrons for input capacitances of 0 and 100 pF are about 295 and 450 respectively (note how there still is noise with zero input capacitance). These values are small relative to the expected 210,000 electrons released per alpha particle. The preamplifier also supplied the bias to the detector via an Ortec 670 power supply. The output of the preamplifier was then connected to an Ortec 570 linear amplifier with variable shaping times, which was then feed into an Ortec Easy MCA-2k for pulse height analysis.

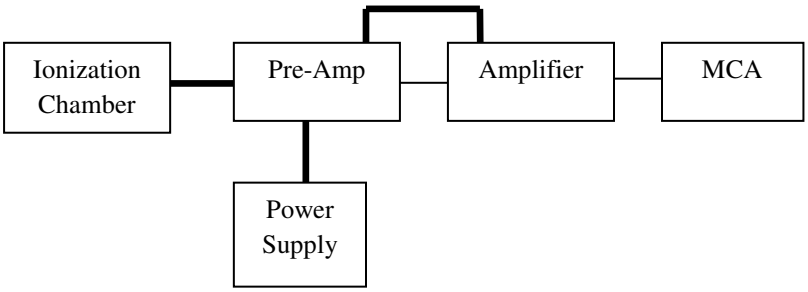



Figure 25: This displays the signal processing system used for measuring the energy of an ionizing particle within the IC

Consideration was taken to ensure the recommended capacitance cables were used and their lengths were as short as possible, specifically at the preamplifier-stage as discussed in Sec. 3.5.2. Also microphonics, which is external vibrations that can cause electrical disturbances in signal processing units, was minimized to the best extent possible by keeping the entire system in its own area and by placing the preamplifier on a type of cushion to reduce vibrations.

### 4.3. Dead Layer

One flaw of the current design of the IC was the *dead layer* that arose from the use of a collimator. A dead layer, in the case of gas-filled detectors, is an area of the detector where ionization is occurring but the electrons created are not being collected. Figure 26 shows the top portion of the IC where the dead layer resides. Because the collimator rests atop the cathode, which is where the electric field "begins" (indicated by the green lines in Figure 26 ), the dead layer has no electric field in which to force the electrons

towards the anode, and therefore a fraction of the total energy from the source is lost in this dead layer.

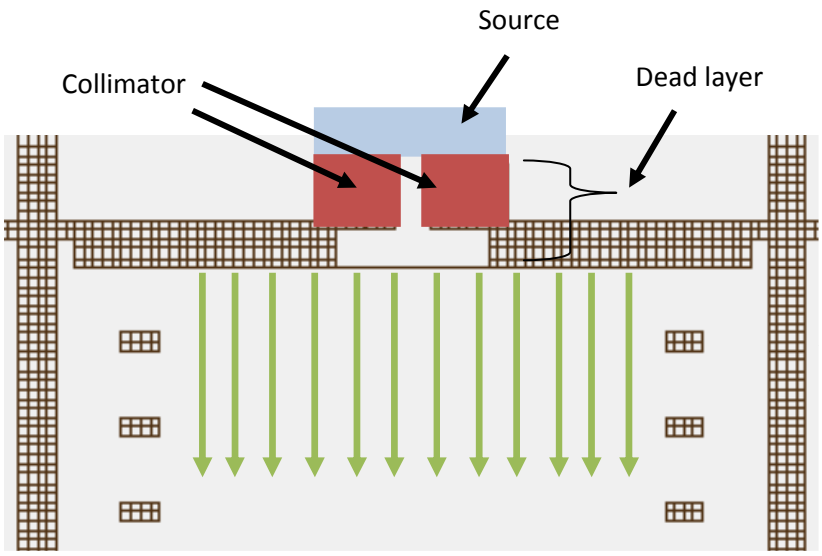



Figure 26: The top portion of the IC displaying the dead layer of the detector, where the green lines indicate the electric field lines.

Because of this dead layer, a correction to the data based on the $dE/dx$ of the particle in the specific gas is needed to accurately predict the energy of an ionizing particle as "seen" by the IC; this correction brings uncertainty in the energy resolution, a highly undesirable feature for our application. It should be noted that even though some of the electrons may naturally diffuse into the chamber and therefore be collected, the time in which they would be collected would statistically not occur when the main signal is being

collected based on the drift times of the particles in the dead layer versus that of the active region of the IC.

The majority of the experiments run on the IC had a dead layer of about 12 mm and therefore large uncertainties, relative to our small energy resolutions, ensued. The main reason for this large dead layer was to allow the use of a much higher activity source, and therefore allow us to characterize one particular variable in weeks rather than months. A brief switch was made to a smaller dead layer, 6.9 mm thick, by using a shorter collimator combined with a smaller diameter aperture. This was done to show that much smaller uncertainties can be obtained, as evident in Figure 27 (the time needed to gather statistically significant data with this collimator increased dramatically). Figure 27 also shows how the data, after being corrected for the differing dead layers, is fairly consistent.

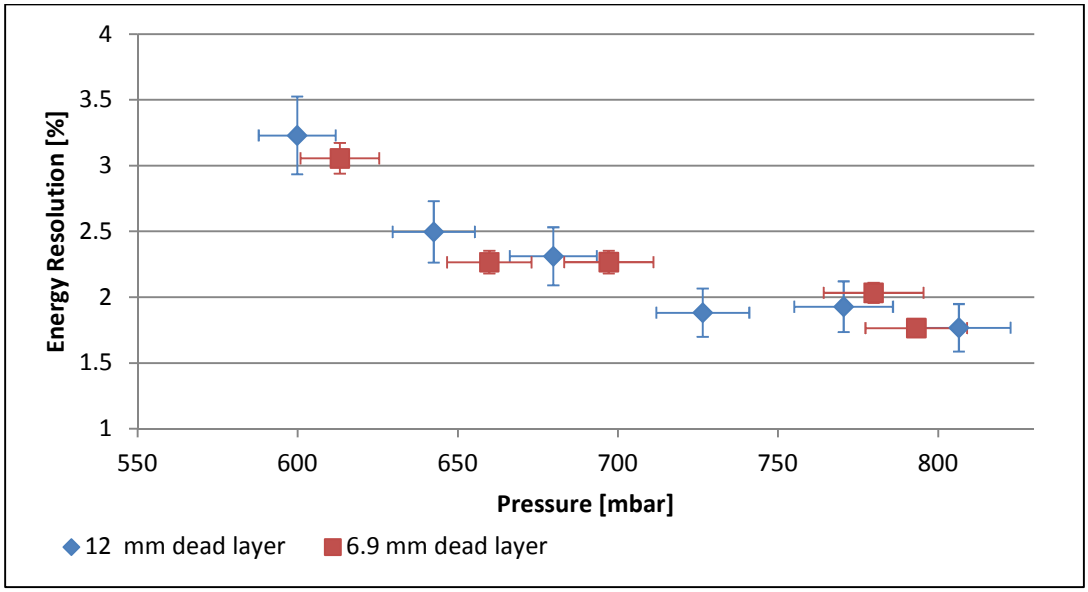



Figure 27: The difference in uncertainties arising for the differing dead layer thicknesses

In the final design of the spectrometer, containing the time-of-flight measurement, no dead layer will occur because all ionizations will occur between the cathode and Frisch grid region of the IC. However some energy loss, and therefore uncertainty, will arise when the particle passes through a thin window which interfaces the vacuum and gas-filled region of the spectrometer (see Sec. 5.5).

### 4.4. Peak Drift

One problem faced when operating ICs is the drift of the measured signal over time. As mentioned in Sec. 2.6.1, small amounts of impurities in the fill gas or the chamber housing the IC can have very detrimental effects on the output signal. As materials naturally outgas, the fill gas becomes more contaminated with various impurities. Specifically, the oxygen in water vapor and air, being highly electronegative, will soak up more and more of the signal electrons as time goes on. With that said, a gradual drift and subsequent broadening in a measured peak is expected due to this natural outgassing from the chamber and IC components themselves. Our IC was initially experiencing significant peak drift which essentially ruined the measured energy resolution, but after a thorough cleaning of the entire IC with ethanol and steel wool, the drift of an alpha peak was reduced to an average value of about $0.08 \pm 0.0009$ %/hr. This was better but still needed to be improved in order to run counts that lasted a day or more. A gas flow was introduced to remedy this.

### 4.5. Gas Flow

The use of a gas flow is another way to combat the natural drift in measured signals from an IC over time. By continually flowing a gas through an IC, the contaminated gas is replaced with non-contaminated gas, and as a result, the concentration of impurities is much lower thus leading to a more stable measured signal. With a gas flow established, the drift of a measured peak from our IC, on average, was reduced to about 0.008 ± 0.0006 %/hr. This reduction in peak drift over time allowed for long counts to not be statistically affected by this phenomenon. In our case, the gas input and output were both controlled by needle valves which allowed a balance between the inflow and the outflow to occur rather easily and precisely. The flow rates used generally refreshed the entire chamber about five times per hour.

A gas flow appeared to be unnecessary as long as new gas was installed periodically. Figure 28 shows how the energy resolution of the IC was comparable whether a gas was flowed or not. The *no flow (fresh gas)* data had newly installed gas during its measurement, before significant contamination was possible, and thus it is expected to be similar to the flowing gas data. A gas flow, therefore, appears to not be a requirement when running short experiments.

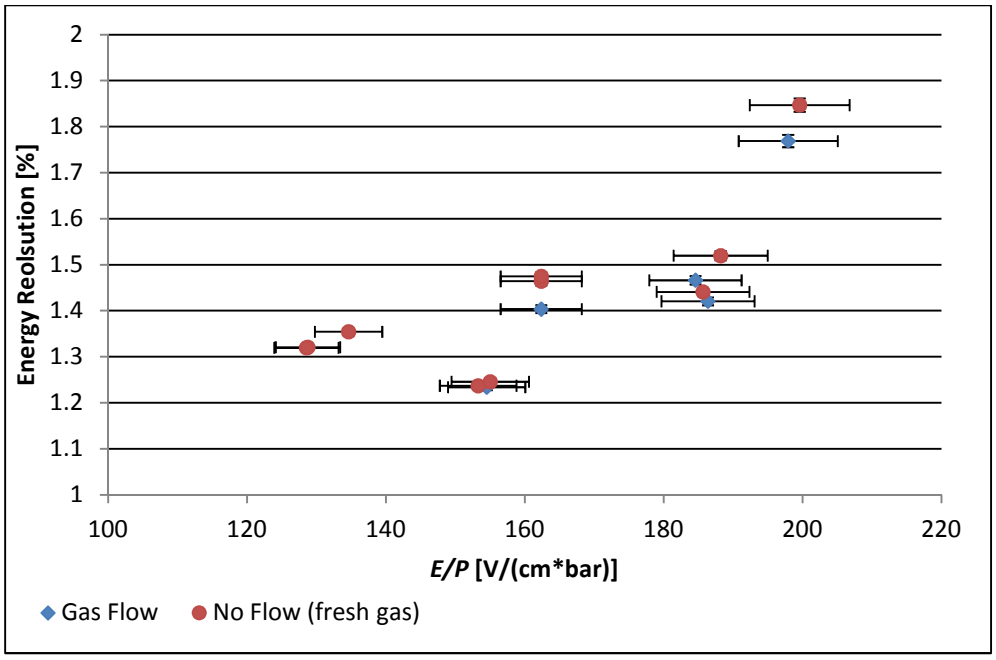



Figure 28: Energy Resolution vs. E/P for gas flow and no gas flow trials

### 4.6. Lateral Acceptance

Another parameter investigated was the lateral acceptance of the IC, that is to say how far off-center can a particle enter the detector yet still deposit its full energy within the detector's active region. To do this, a highly collimated source was simply moved in small increments off-center, and the ensuing peak was analyzed. Figure 29 shows how the count rate significantly drops off as the particle exceeds about 10 mm from the center of the IC. This indicates that a large portion of the particles are not depositing their full amount of energy and thus not being measured in the peak, but at lower energies. Likewise, Figure 30 looks at the FWHM of the peak as a function of the source's position from center. One sees the FWHM increasing as when one gets further away from the center. This is another indication that the ionizing particles are not depositing its full energy.

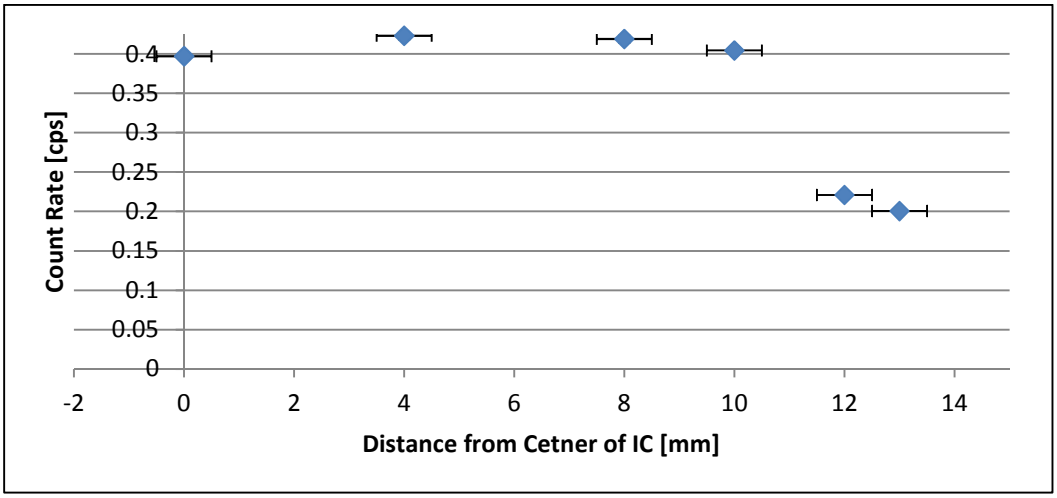



Figure 29: The count rate of the source as a function of its distance from center the IC

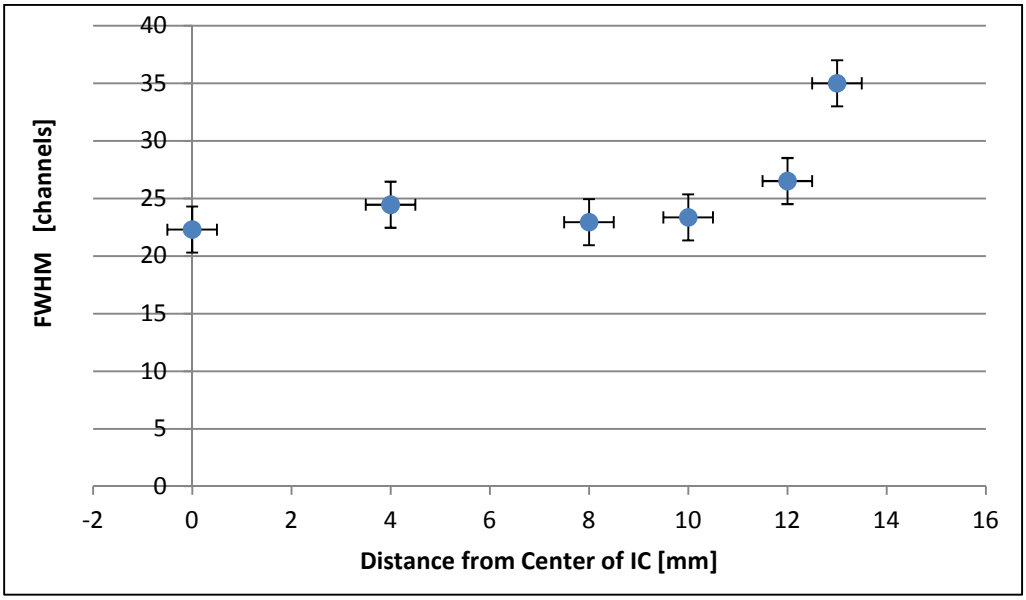



Figure 30: The FWHM of an alpha peak as a function of the distance the source is from the center of the IC

### 4.7. Shaping Time

Another major variable investigated was the shaping time of the linear amplifier. The shaping time is an important parameter for ICs because the drift time of electrons in most cases is on the order a few μs and so too are the shaping times of most linear amplifiers. In other detectors, e.g. solid state detectors, the "drift time" is much less than typical shaping times and it therefore has less significance. The shaping time is also a fundamental component in Bragg curve spectroscopy. As stated in Sec. 2.5, the shaping time can be thought of as the time in which the linear amplifier is actually collecting a signal. Therefore, in order to measure the full signal, the shaping time must be much greater than the temporal width of the signal. However, one must not set an arbitrarily high shaping time because of the resulting increases in pulse pile-up and electronic noise.

The main contributions of noise can be categorized into two groups, series and parallel noise [Knoll]. Series (e.g. Johnson or thermal noise) and parallel noise (e.g. leakage current) are sources of noise that are in series or parallel with the input signal respectively. As shown below in Figure 31, when the shaping time is increased the contribution from series noise decreases while the contribution from parallel noise increases. This effect produces a minimum value of the noise with respect to shaping time and should be taken into consideration when selecting the optimum shaping time for any experiment.

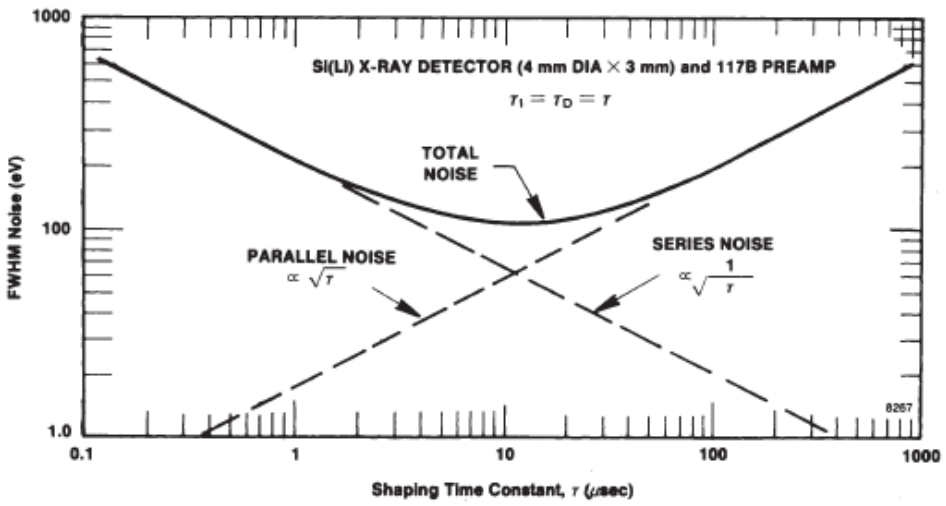



Figure 31: The series and parallel noise contributions as a function of shaping time [Ametek]

Figure 32 shows the channel number of an alpha peak as a function of the electric field to pressure ratio, *E/P*, in the cathode-Frisch grid region of the IC at various shaping times. Saturation in channel number at each *E/P* value is achieved when the shaping time is greater than or equal to 2 μs. This is in line with the drift times of the electrons, based on Figure 8 and the dimensions of the IC, being about 1.8-2.3 μs.

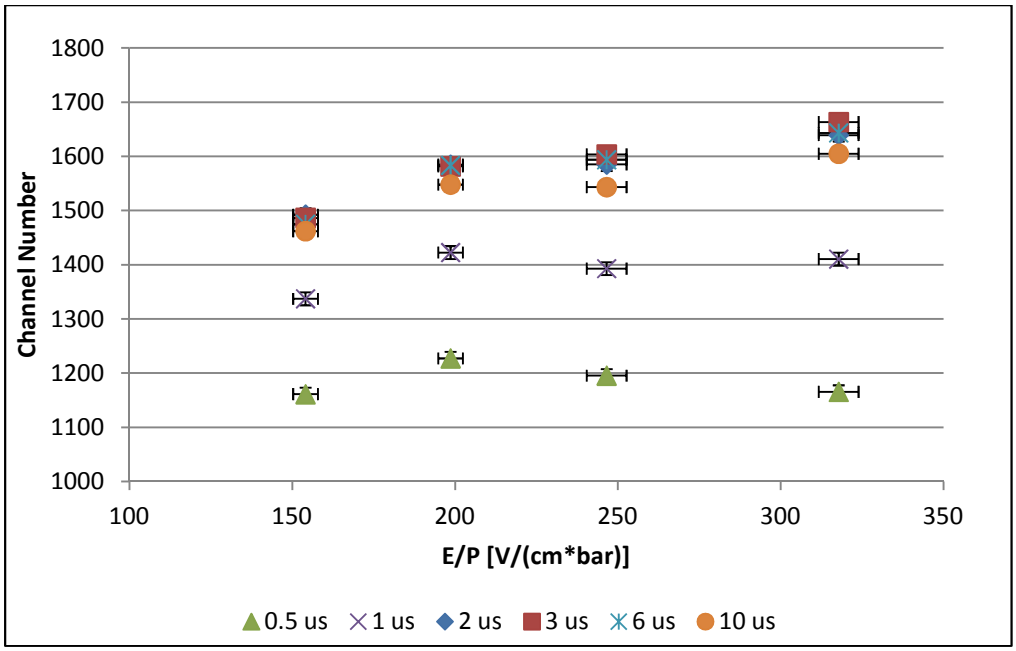



Figure 32: Channel number vs. *E/P* at various shaping times

If we turn our attention to Figure 33, we see the energy resolution as a function of the shaping time. The point here is that even though roughly the same amount of charge is collected at each shaping time, as evident from Figure 32, the energy resolution is significantly different. Because of the relationship between energy resolution and number of electrons (Eq. 9), this behavior is not expected but could be explained by the series and parallel noise contributions to the signal. The drift time at the *E/P* value used for the data in Figure 33 is estimated to be about 2.2 μs, so a 2 μs shaping time does not represent the fully collected charge, and therefore the energy resolution at 2 μs is not ideal. The divergence of the energy resolution at 6 and 10 μs could be possibly explained by the fact that we are deviating from the minimum of Figure 33.

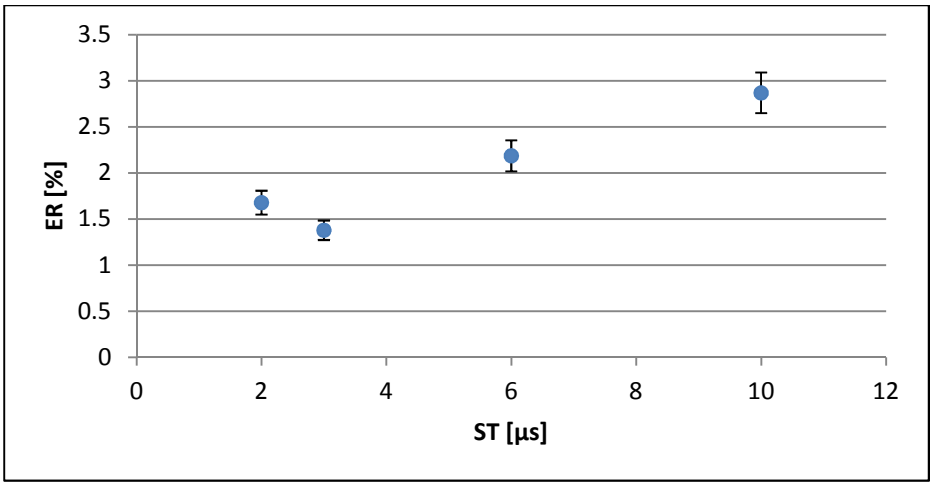



Figure 33: The energy resolution as a function of shaping time

Depending on the drift velocity of the electrons in the IC, the drift time of the electrons can range from 1.8-2.3 µs and it consequently warrants a look into how the energy resolution changes as a function of the shaping time. Figure 34 shows a comparison of the energy resolution as a function of *E/P* at both 2 and 3 µs shaping times. If one correlates the *E/P* value to the drift velocity of the electrons, their subsequent drift time is predicted to be less than 2 µs for *E/P* values between about 100 and 270 *V/(cm*bar)*. In that *E/P*-range, the energy resolution of the IC at 2 µs is shown to be superior to that at 3 µs. However, when we deviates from that range, on either side, a switch occurs where now the 3 µs shaping time becomes the better measure. The point being, if one is operating at a shaping time smaller then the temporal width of the signal, then one is obviously not measuring the full signal and a fluctuation in the measured signal is expected; this would in turn lead to a poorer energy resolution. On the other hand, if one is using a shaping time larger than the width of the signal (not too much larger) then one should be collecting the full amount of charge every time, with no fluctuations (not

accounting for the natural fluctuation due to statistics of ionization), leading to better energy resolution.

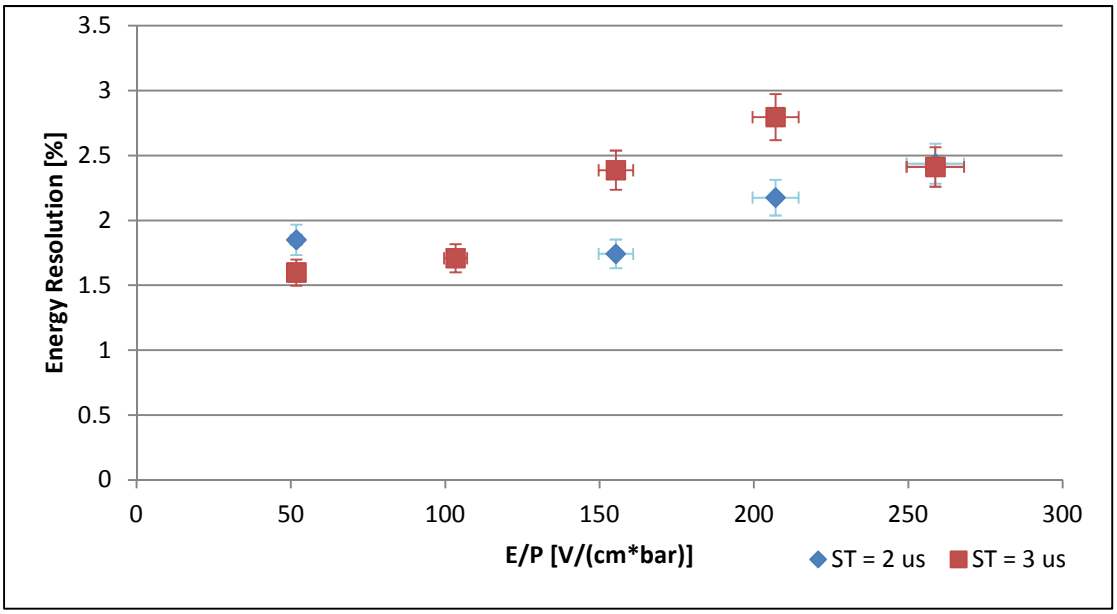



Figure 34: Energy resolution vs. E/P at 2 and 3 μs shaping times

In summary, the shaping time is working as expected but adds another variable to the functionality of the IC because the energy resolution is a sensitive function of shaping time. In the final assembly of the entire spectrometer, isobutane will be the fill gas used. Not only does isobutane exhibit a higher drift velocity for electrons (reducing electron capture), it also shows a saturation in the drift velocity at higher *E/P* values, where then small changes in the *E/P* value should not have drastic effects on the electron drift time. At that point, the shaping time will not have the effect shown in Figure 34.

### 4.8. Electric Field

As mentioned in Sec. 2.3.3, an IC is operated in the saturation region of Figure 3. Figure 35 displays a similar graph of the channel number of an alpha peak (proportional to the total charge collected) vs. the electric field in the cathode-Frisch grid region at two different pressures.

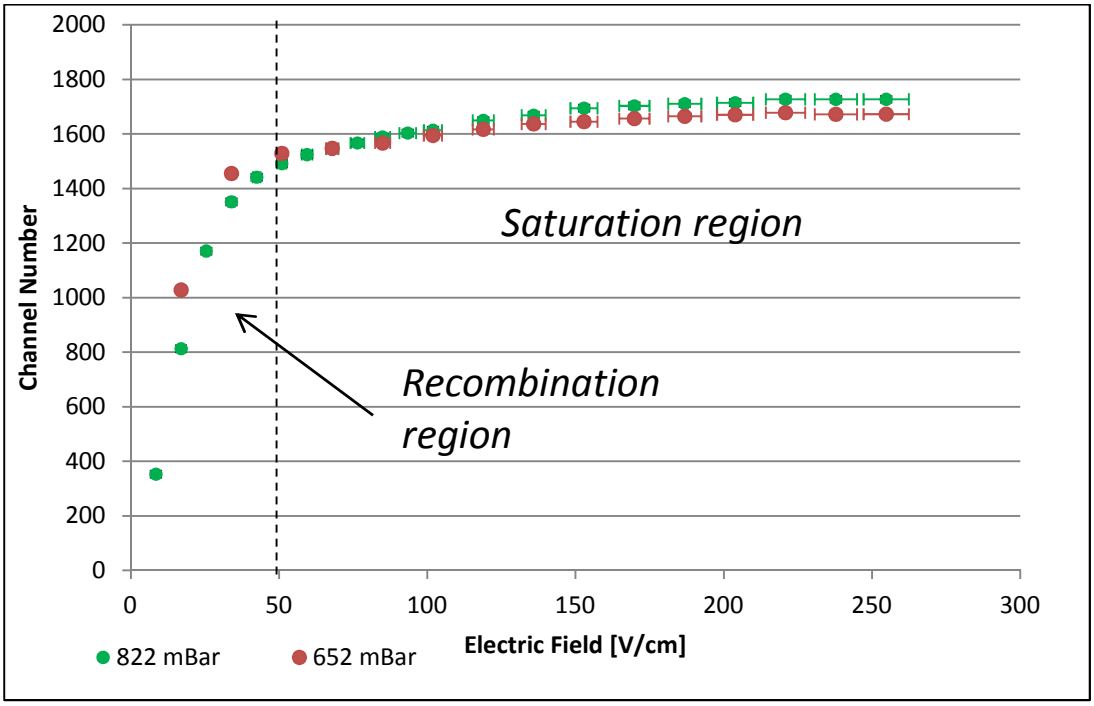



Figure 35: The I-V curve of our IC

As expected, the total charge collected changes considerably in the recombination region of the above I-V curve. This region, is followed by the *saturation region* which occurs above about 50 *V/cm* for both pressures investigated. This saturation, as previously described, is due primarily to the fact that the electrons now have enough energy to largely overcome electron capture and recombination. Figure 35 is indicative of correctly working IC.

If we turn our attention to the energy resolution as a function of the electric field in the cathode-Frisch grid region, we see a fairly constant energy resolution over a wide range of electric field values (Figure 36). This is expected simply because the IC is being operated in the saturation region, where the full amount of charge is being collected and no alterations occur with larger electric fields.

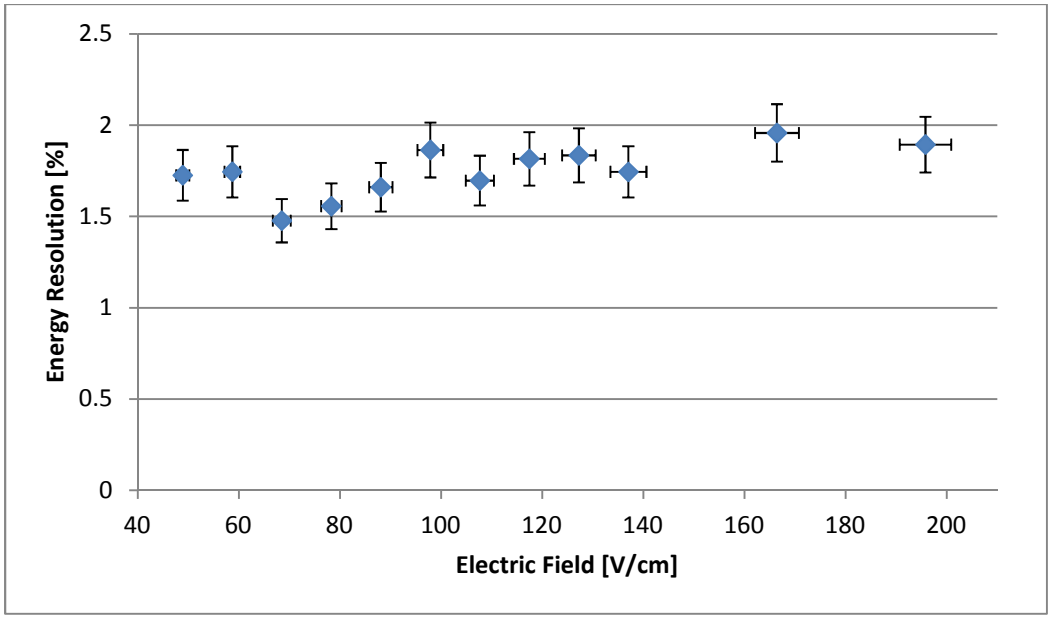



Figure 36: The energy resolution as a function of applied electric field in the cathode-Frisch region of the IC

Eq. 34 states how the ratio of electric field in the Frisch grid-anode region to the electric field in the cathode-Frisch grid region must be greater than some condition (approximately unity) so as to avoid the grid wires of the Frisch from capturing some of the signal electrons as they pass by. Figure 37 shows the affect the different electric field ratios have on the measured signal. As expected, when the ratio is less than unity, the

measured signal size is significantly decreased, about 14% smaller with a ratio of 0.7. When this ratio is above unity, the signal is fairly consistent.

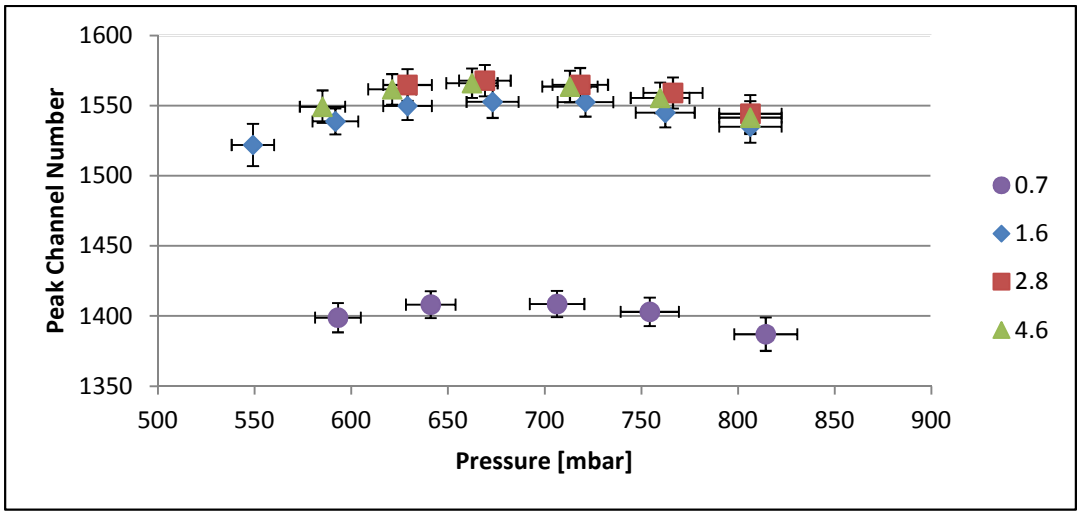



Figure 37: Channel number of the Pu-239 alpha peak as a function of pressure for different ratios of the Frisch grid-anode to cathode-Frisch grid electric fields

### 4.9. Pressure

One of the more interesting parameters in the operation of an IC is the gas pressure due to its give-and-take effects on the overall performance of the IC. For instance, an increase in pressure has an obvious increase in recombination (Eq. 16). This leads to a lower amount of total electrons collected, thus worsening the best achievable energy resolution. On the other hand, with a higher pressure the anode is better screened because of the ionizing particle's shorter range, and thus the signal derived from the Frisch grid-anode region would more accurate. The pressure's natural correlation with the drift velocity, and therefore electron capture, can also not be forgotten. This section will look at the pressure dependence on the performance of the IC.

Figure 38 shows the measured signal as a function of pressure for two alpha particles with different energies. The dotted and solid lines in the figure refer to the estimated pressure in which the 5486 and 5156 keV alpha particles, respectively, would hit the Frisch grid. This is an undesirable condition, for one wants all ionizations to occur before the Frisch grid, and therefore the IC should not be operated below or near this pressure for these energy alpha particles. In Figure 38 one can see how over a 200 mbar change in pressure has small effects on the overall measured signal; this indicates that small changes in pressure or temperature should have negligible effects on the performance of the IC. This is expected simply because the only thing different when the IC is operated at lower pressures is that the particles are traveling further distances into the detector.

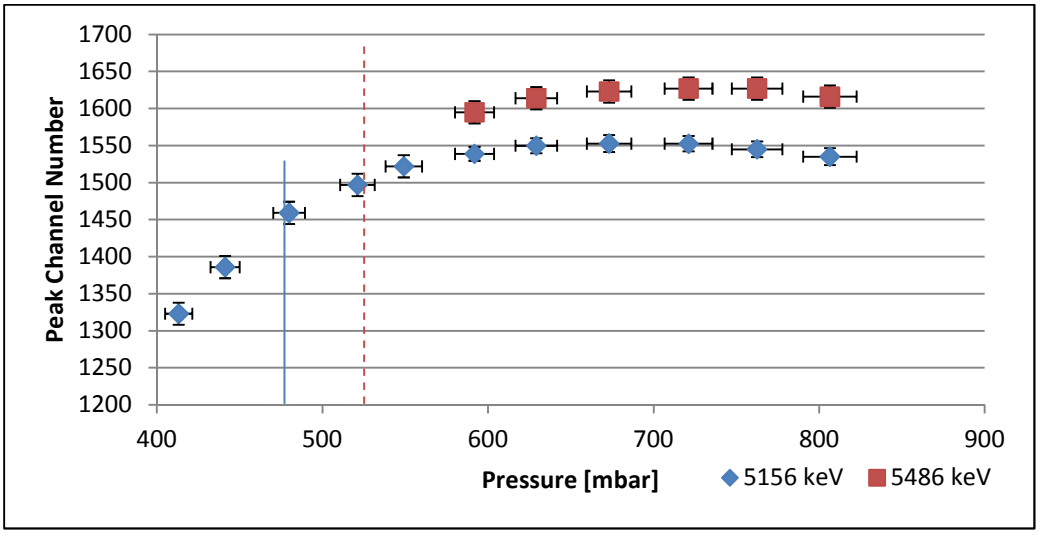



Figure 38: The channel number of an alpha peak as a function of pressure for two alpha particles of different energies

Figure 39 shows the energy resolution of the IC as a function of pressure. A gradual increase, and therefore worsening, in the energy resolution is seen with decreasing pressure until a possible saturation occurs. This figure was replicated many times. One possible explanation for this poorer resolution at lower pressures is that some of the alpha particles may be leaving the chamber without depositing their full energy because of their increased range. However, Figure 38 alleviates this concern by showing a saturation in the measured signal at the range of pressures displayed in Figure 39; SRIM simulations also corroborate the hypothesis. Another concern could be that some of the signal electrons, born from the alpha particle ionizations, are exiting the chamber through the guard rings. A more in depth simulation code would be needed to shed light on the actual paths the electrons take within the IC. A much larger IC could be used to remove the concern altogether.

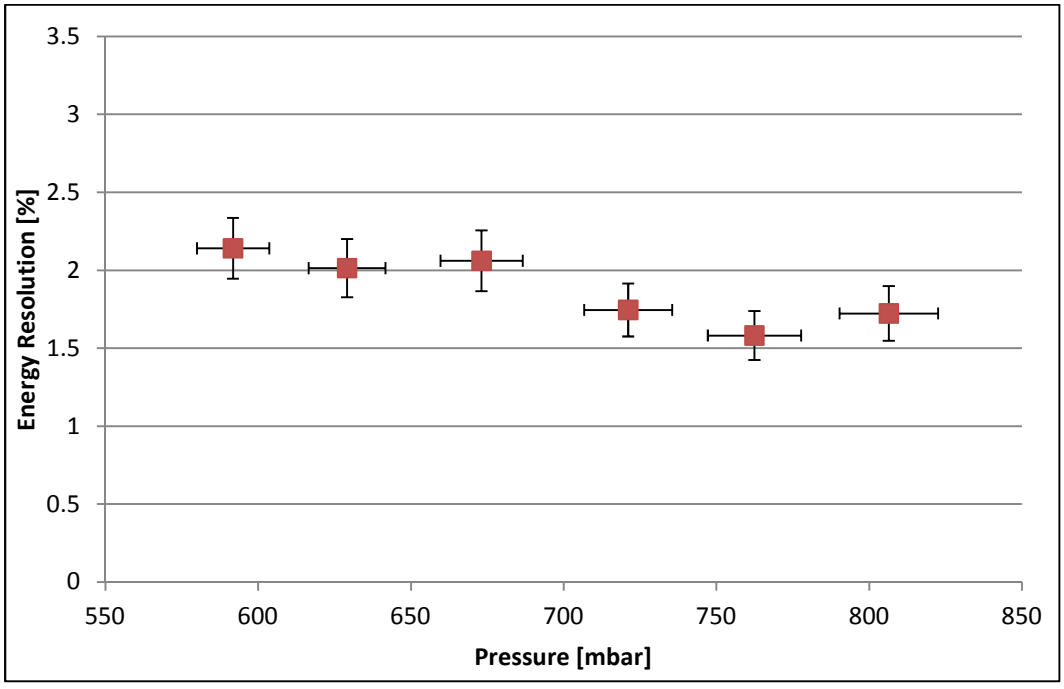



Figure 39: The energy resolution as a function of pressure

### 4.10. Bragg Curve Spectroscopy

As discussed in Sec. 2.5, the main way of extracting Bragg peak information from an IC is by using a linear amplifier with a shaping time that is short relative to the entire temporal width of a signal. Figure 40 shows a comparison of two histograms, counts vs. energy, of the peaks generated by alpha particles of three different energies (note that both figures are from the same trial with the signal being split to two different multi channel analyzers). The figure on the left uses a linear amplifier with a large shaping time of 3 μs, whereas the figure on the right uses a short shaping time of 0.5 μs. The left figure is indicative of the total energy of the three different alpha particles, shown by three distinct peaks, while the right figure is indicative of just the beginning of the Bragg curve, i.e. the Bragg peak, of the three alpha particles. This shows how three different alpha particles give rise to the same Bragg peak, which is representative of their same atomic number.



Figure 40: Counts vs. energy graphs of the peaks generated from a source containing three alpha particles of different energy for a linear amplifier with a shaping time of 3 μs (left) and 0.5 μs (right)

# Chapter 5

# Conclusions and Future Work

---

## 5.1. Conclusions

Many of the pertinent variables which dictate the functionality of an ionization chamber have been discussed, measured, and their implications analyzed. More importantly, most of the parameters' behavior seemed to be consistent with basic theory. For our IC, a gas flow was shown to allow one to run very long experiments without significant peak drift occurring. The lateral acceptance, indicating how far off center a particle can enter the detector and give meaningful results, was about ±10 mm. The electric field functioned exactly as expected, where the energy resolution was fairly constant over a wide range of values. The pressure, alternatively, gave poorer energy resolution when the chamber was operated at lower pressures, and this effect should be further investigated.

The lowest energy resolution obtained was just under 1.5% when corrected for the dead layer, and was just above our desired goal of 1.0-1.25%. To reach the desired goal for the entire spectrometer of a less than one *amu* for both the heavy and light fission fragment, a further improvement in the energy resolution of the ionization chamber is needed. The initial atomic number measurements show promise, yet more resources are needed to fully test this functionality.

### 5.2. Energy Resolution

A few tests to better the energy resolution of the IC revolve around the electronic noise of the system. First, by increasing the Frisch gird-anode distance the input capacitance at the preamplifier input will be reduced. Second, placing a specific-value capacitor between the Frisch grid and anode will reduce some of fluctuations in the voltage from the power supply along with some high frequency noise. Both of these acts are designed to reduce the noise sent to the preamplifier and could improve the IC's energy resolution by eliminating small fluctuations in the measured signal.

### 5.3. Pressure Dependence

A more detailed investigation into the effects of pressure on the operation of the IC should be performed because this behavior seems to be inconsistent. To investigate lower pressures, one would not only need to make the IC longer, because particles travel further at lower pressures, but also wider; this would require rebuilding the IC. Although its current geometrical state is satisfactory for the use of fission fragments because they travel much shorter distances, to alleviate *any* concerns of ionizing particles not depositing their full energy or the signal electrons leaving the IC, a wider IC would be necessary.

### 5.4. Isobutane

The fill gas used for the entirety of the experiment was P-10 due to its inexpensiveness, however many groups have used the more expensive isobutane gas instead. Although they both have similar W-values for alpha particles [Bay] isobutane has a much larger

stopping power meaning the same length chamber can be operated at much lower pressures because the particles will travel shorter distances. This allows one to better quantify the pressure dependence of the IC without rebuilding the entire IC. Also, slightly better energy resolution with isobutane is generally seen [Adhikari].

### 5.5. Window

In the final design of the 2v-2E spectrometer, the time-of-flight measurement must be coupled to the IC's energy and atomic number measurement. Because the former measurement occurs in a high vacuum environment, an interface between that and the IC's gaseous environment is needed. A thin Mylar window is one of the more commonly used choices for this interface. However, recently silicon nitride windows have been used due to superior energy straggling for heavy ions [Döbeli]. A design used to hold the window, pressure tests on the window, and a slight modification of the IC's support structure will be needed to connect the IC to the time-of-flight portion of the spectrometer and therefore fully assemble one arm of the 2v-2E spectrometer.

## References


Adhikari, S.; Basu, C.; et al., 2006. Performance of an Axial Gas Ionization Detector. *IEEE Transactions on Nuclear Science,* August, 53(4), pp. 1-19.

Ahmed, S. N., 2007. *Physics and Engineering of Radiation Detection.* 1st ed. San Diego: Elsevier.

Al-Adili, A.; Hambsch, F.-J.; et al., 2012. On the Frisch-Grid Signal in Ionization Chambers. *Nuclear Instruments and Methods in Physics Research A,* Volume 671, pp. 103-107.

Ametek, *Introduction to Amplifiers.* [Online]. Available at: www.ortec-online.com

Ammi, H.; Chekirine, M., 1996. Electronic Collimation for Precise Measurment of Resolution with a Gridded Ionization Chamber. *Vacuum,* Volume 47, pp. 33-34.

Barrette, J.; Braun-Munzinger, P.; Gelbke, C. K., 1975. ΔE-E Telescope for the Identification of Heavy Ions at Low Energies with Good Energy Resolution and Optimum ΔE Resolution. *Nuclear Instruments and Methods,* Volume 126, pp. 181-187.

Bay, Z.; McLernon, F. D., 1965. Absolute Measurement of W for Polonium-210 Alpha Particles in Nitrogen, Argon, and an Argon-Methane Mixture. *Radiation Research,* Janurary, 24(1), pp. 1-8.

Bertonlini, G., 1984. Alpha Particle Spectroscopy by Gridded Ionization Chamber. *Nuclear Instruments and Methods in Physics Research,* Volume 223, pp. 285-289.

Blum, W.; Reigler, W.; Rolandi, L., 2008. *Particle Detection with Drift Chambers.* 2nd ed. Berlin: Springer-Verlag.

Bocquet, J. P.; Brissot, R.; Faust, H. R., 1988. A Large Ionization Chamber for Fission Fragment Nuclear Charge Identification at the Lohengrin Spectrometer. *Nuclear Instruments and Methods in Physics Research A,* Volume 267, pp. 466-472.

Böhm, J., 1976. Saturation Corrections for Plane-Parallel Ionization Chambers. *Physics in Medicine and Biology,* 21(5), pp. 754-759.

Boucheneb, N.; Asghar, M.; et al., 1991. A High-Resolution Multi-Parametric Study of $^{239}Pu(n_{th},f)$ with the Cosi-Fan-Tutte Spectrometer. *Nuclear Physics A,* Volume 535, pp. 77-93.

Boucheneb, N.; Geltenbort, P.; et al., 1989. High-Resolution Measurments of Mass, Energy, and Nuclear Charge Correlations for $^{229}Th(n,f)$ with the COSI FAN TUTTE Spectrometer. *Nuclear Physics A,* Volume 502, pp. 261-270.

Brookhaven National Laboratory, 1952. [Online]. Available at: http://www.nndc.bnl.gov/

Brown, M. A.; Biondi, S., 1949. *Measurment of Electron-Ion Recombination,* Cambridge: Massachusetts Institute of Technology Research Laboratory of Electronics.

Bunemann, O.; Cranshaw, T. E.; Harvey, J. A., 1949. Design of Grid Ionization Chambers. *Canadian Journal of Research,* 27(A), pp. 191-206.

D'Erasmo, G.; Paticchio, V.; Pantaleo, A., 1985. A Transmission Time Detector for Low Energy Light Ions. *Nuclear Instruments and Methods in Physics Research A,* Volume 234, pp. 91-96.

Döbeli, M.; Kottler, C.; et al., 2004. Gas Ionization Chambers with Silicon Nitride Windows for the Detection and Identification of Low Energy Ions. *Nuclear Instruments and Methods in Physics Research B,* Volume 219-220, pp. 415-419.

Göök, A.; Hambsch, F.-J.; et al., 2012. Application of the Shockley-Ramo Theorem on the Grid Inefficiency of Frisch Grid Ionization Chambers. *Nuclear Instruments and Methods in Physics Research A,* Volume 664, pp. 289-293.

Göök, A., 2008. *Investigations of the Frisch-grid Inefficiency by Means of Wave-form Digitizer.* Örebro: Öbero University.

Gruhn, C. R.; Binimi, N. M.; et al., 1982. Bragg Curve Spectroscopy. *Nuclear Instruments and Methods,* Volume 196, pp. 33-40.

Hagiwara, M.; Sanami, T.; et al., 2008. Extension of Energy Acceptance of Bragg Curve Counter at High-Energy End. *Nuclear Instruments and Methods in Physics Research A,* Volume 592, pp. 73-79.

(ICRU) International Commision on Radiation Units and Measurements, 1979. *ICRU Report 31: Average Energy Requried to Produce an Ion Pair,* Washington D. C.: ICRU.

Kapoor, S. S.; Ramamurthy, V. S., 1986. *Nuclear Radiation Detectors.* 1st ed. New Delhi: New Age International (P) Ltd.

Khryachkov, V. A.; Dunaeva, I. V.; et al., 2003. A Method for Rapid Measurements of Working-Gas Properties in a Pulse Ionization Chamber. *Instruments and Experimental Techniques,* 46(6), pp. 804-813.

Knoll, G. F., 2000. *Radiation Detection and Measurement.* 3rd ed. New Jersey: John Wiley & Sons.

Koczon, P.; Mutterer, M.; et al., 1987. Cold and "Hot" Fragmentation in Thermal Neutron Induced Fission of $^{245}$Cm. *Physics Letters B,* 191(3), pp. 249-252.

Kosev, K. M., 2007. *A High Resolution Time-of-Flight Spectrometer for Fission Fragments and Ion Beams.* Dresden.

Kozulin, E. M.; Bogachev, A. A.; et al., 2008. The CORSET Time-of-Flight Spectrometer for Measuring Binary Products of Nuclear Reactions. *Instruments and Experimental Techniques,* 51(1), pp. 44-58.

Masayuki, K.; Kikuchi, J.; Doke, T. Y., 1979. Fano Factor in Gas Mixture of Ar+10% $CH_4$. *Nuclear Instruments and Methods,* Volume 163, pp. 289-291.

Melton, C.; Hurst, G.; Bortner, T., 1954. Ionization Produced by 5-MeV Alpha Particles in Argon Mixtures. *Physical Review,* 1 November, 96(3), pp. 643-645.

Muller, A.M.; Dobeli, M.; et al., 2012. Performance of ETH Gas Ionization Chamber at Low Energy. *Nuclear Instruments and Methods in Physics Research B,* Volume 287, pp. 94-102.

Ochiishi, H.; Ito, H.; et al., 1996. Application of Bragg-Curve Counters to Target Multifragmentation Measurement. *Nuclear Instruments and Methods in Physics Research A,* Volume 369, pp. 269-276.

Oed, A.; Geltenbort, P.; et al., 1983. High Resolution Axial Ionization Chamber for Fission Products. *Nuclear Instruments and Methods,* Volume 205, pp. 455-459.

Parker Jr., J. H.; Lowke, J. J., 1969. Theory of Electron Diffusion Parallel to Electric Fields. 1. Theory. *Physical Review,* 181(1), pp. 290-301.

Sanami, T.; Hagiwara, M.; et al., 2008. A Bragg Curve Counter with an Active Cathode to Improve the Energy Threshold in Fragment Measurements. *Nuclear Instruments and Methods in Physics Research A,* Volume 589, pp. 193-201.

Sanami, T.; Hagiwara, M.; et al., 2009. A Bragg Curve Counter with an Internal Production Target for the Measurement of the Double-Differential Cross-Section of Fragment Production Induced by Neutrons at Energies of Tens of MeV. *Nuclear Instruments and Methods in Physics Research A,* Volume 610, pp. 660-668.

Sauli, F., 1977. *CERN 77-09: Principles of Operation of Multiwire Proportional and Drift Chambers,* Geneva: CERN.

Schillebeeckx, P.; Wagemans, C.; et al., 1994. Investigation of Mass, Charge and Energy of $^{241}Pu(n_{th},f)$ Fragments with the Cosi-Fan-Tutte Spectrometer. *Nuclear Physics A,* Volume 580, pp. 15-32.

Skullerud, H. R., 1969. Longitudinal Diffusion of Electrons in Electrostatic Fields in Gases. *Journal of Physics B: Atomic and Molecular Physics,* 2(2), pp. 696-705.

Starzecki, W.; Stefanini, A. M.; et al., 1982. A Compact Time-Zero Detector for Mass Identification of Heavy Ions. *Nuclear Instruments and Methods,* Volume 193, pp. 499-505.

White, M. C., 2011. *Advancing the Fundamental Understanding of Fission.* Los Alamos: Los Alamos National Laboratory.

Wilkinson, D., 1950. *Ionization Chambers and Counters.* 1st ed. Cambridge: The University Press.

Wiza, J. L., 1979. Microchannel Plate Detectors. *Nuclear Instruments and Methods in Physics Research,* Volume 162, pp. 587-601.

Ziegler, J. F., *Particle Interactions with Matter.* [Online]. Available at: www.SRIM.org.

## List of Appendices

**Appendix A – Charge Sensitive Preamplifiers** ..... **84**

A.1. Properties ..... 84

A.2. Bragg Curve Spectroscopy ..... 85

**Appendix B – Current and Pulse Mode of Ionization Chamber Operation** ..... **87**

B.1. Introduction ..... 87

B.2. Pulse Mode ..... 87

B.3. Current Mode ..... 88

## Appendix A

## Charge Sensitive Preamplifiers

---

### A.1. Properties

The signals produced from gas-filled detectors are generally very small where the currents can be on the order of $10^{-9}$ A, and therefore in most applications signal processing becomes a necessity. Usually a preamplifier is connected directly after the detector to ready the signal for further amplification and signal processing. If noise is generated in the detector or its cabling, this noise, like the actual signal, will be passed onto the preamplifier where it will also undergo the future signal processing thus altering the true signal measured by the IC. For that reason, eliminating the noise before or at the preamplifier stage is vital. It bears briefly mentioning how the commonly used preamplifiers for ionization chambers (IC), charge sensitive preamplifiers, function.

In many preamplifiers the output voltage, $V_{out}$, is proportional to the capacitance of the detector, $C_d$. This capacitance can fluctuate for a variety reasons such as the small changes in applied voltage, temperature, microphonics, etc. For ICs aiming for very high energy resolution, these effects can be very damaging and there removal is needed. Charge sensitive preamplifiers accomplish this, in short, by integrating the total charge from the detector across a feedback capacitor which then produces a voltage across a feedback resistor; it is this voltage which is ultimately measured. This process removes the dependence of the signal on $C_d$. To ensure that all the charge from the detector actually reaches the feedback capacitor, Ahmed (Ahmed) explains why $C_f >> C_{in}$ ($C_f$and

$C_{in}$ being the feedback and input capacitances respectively). It should also be noted that the value of $C_{in}$ also contributes to the noise of the system and is thus another reason why it should be minimized (e.g., short cables).

### A.2. Bragg Curve Spectroscopy

One unique feature when using charge sensitive preamplifiers to measure a signal from an IC is that the time profile of a signal is preserved. That is to say, the rise time of a signal generated by a charge sensitive preamplifier is indicative of the temporal width of a signal as it drifts though the detector. Figure 41 shows the beginning portions of a typical voltage pulse from our charge sensitive preamplifier via an oscilloscope. One can see how the voltage initially rises, stopping when all the charge is collected, and then begins to decay predictably based on RC time constant of the preamplifier. One can think of the initial rise in voltage being detector, or signal, dependant and the subsequent fall in the voltage being preamplifier dependant.

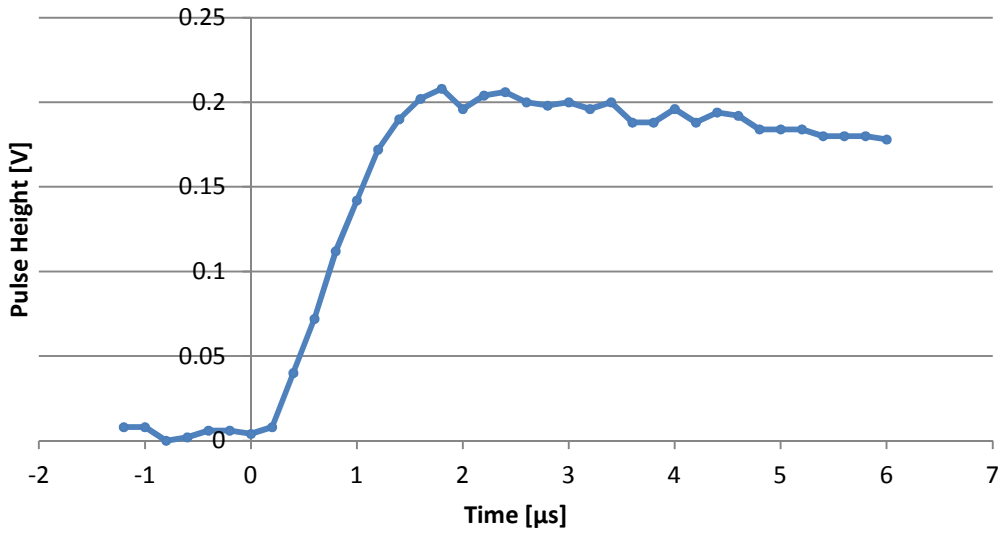



Figure 41: A typical voltage pulse as a function of time as measured from an IC connected to a charge sensitive preamplifier

As discussed in Sec. 2.5, to measure just the Bragg peak of a Bragg curve, one wants to measure just the beginning portions of the signal as opposed to the entire signal. In this case, one uses a small shaping time relative to the temporal width of the signal within the chamber. Because charge sensitive preamplifiers preserve this temporal width of the signal, which one can relate to the spatial width of the signal via the drift velocity of the electrons, one now has a measure of the range of an ionizing particle. For that reason, by using variable shaping times one can measure certain portions of the Bragg curve and now gain atomic charge information.

## Appendix B

## Current and Pulse Mode of Ionization Chamber Operation

---

### B.1. Introduction

Ionization chambers (IC), like most other radiation detectors, can be operated in either pulse mode or current mode. In pulse mode a voltage pulse is measured, whereas in current mode it is the average current being measured. Their differences and the common applications in which each is generally used are described below.

### B.2. Pulse Mode

When detectors are operated in pulse mode, the amplitude and timing of *each individual* event, which occur in the detector, can be determined [Knoll]. Pulse mode is generally the mode of operation in spectroscopy applications where each ionizing radiation is to be analyzed in detail. Figure 42 shows the basic electronic layout of an IC operating in pulse mode. The two electrodes are biased to some potential, $V_b$,where $R$ is the resistance of a resistor, $C$ is the capacitance of the detector and other stray capacitance, and $V_{out}$ is the output voltage being measured. $V_{out}$ can be thought of as an induced change in $V_b$. If there is no change in $V_b$ then $V_{out}$ is zero.

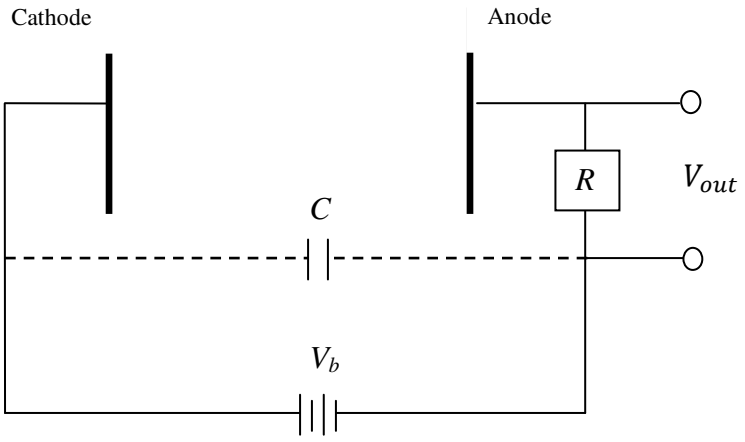



Figure 42: An ionization chamber operating in pulse mode

Initially when no ionizing radiation has entered the chamber, no charge has been produced to alter $V_b$ and therefore $V_{out}$ is zero (see Sec. 3.3 to understand how $V_{out}$ is actually produced). When ionizing radiation enters the chamber, a change in $V_b$ occurs and $V_{out}$ is readout across the resistor. The important point to note about most radiation detectors operating in pulse mode, and ICs are no exception, is that $V_{out}$ is produced for *every* event and is therefore a measure of each ionizing radiation event.

### B.3. Current Mode

A detector operating in current mode simply measures the current produced by a set of ionizing radiations. Because of the fact that current, which is defined as the rate of change of charge over time, is the quantity being measured here, ICs run in current mode produce an *average value* with respect to time. In pulse mode one is gaining a measurement for every single event, while in contrast, current mode looks at a group of events. Current mode is generally used in applications where the specific pulse height of

each event is not desired, just the total pulse height from a group of events (e.g. Geiger counters where only the *presence* of radiation is desired not its specific characteristics).

The basic circuitry of an IC operating in current mode uses some type of ammeter, or ammeter-equivalent circuit, to measure the ionization current. There are several ways to measure the current (see [Knoll]), but they mostly all involve collecting a signal about an *RC*-circuit where the value of *RC*, being the product of the resistance and capacitance of a resistor and capacitor respectively, is assumed to infinite relative to the drift time of the signal within the IC.